7.4.3 *Rabbit Models for Infectious Diseases and Deficiency of Immunological System*

Manabe et al. (Manabe et al. 2008) showed that New Zealand white rabbits are useful animal for human latent tuberculosis. The global epidemic of tuberculosis claims more than two million lives yearly. *Mycobacterium tuberculosis* latently infects one third of the world population. They examined aerosol-infected rabbits with *Mycobacterium tuberculosis* and showed the formation of caseous lung granulomas which are strikingly similar to tuberculous lung lesions in humans. The lung burden of infection peaked at 5 weeks after aerosol infection followed by a host containment of infection that occurred in all rabbits. Corticosteroid-induced immunosuppression initiated after the disease containment resulted in a reactivation of disease. They also characterized the lung cellular immune response to inhaled *Mycobacterium tuberculosis* in the susceptible inbred Thorbecke rabbit (the genomically sequenced strain) and compared it to outbred, *Mycobacterium tuberculosis*-resistant, New Zealand white rabbits (Mendez et al. 2008). The development and severity of the immune reconstitution inflammatory syndrome was dependent on the antigen load at the time of immunosuppression and the subsequent bacillary replication during the corticosteroid-induced immunosuppression. This corticosteroid model is the only animal model to study the immune reconstitution inflammatory syndrome. The lung granulomas of inbred rabbits had a significantly higher number of cells expressing MHC Class II and CD11b, and a lower number of CD8 + T cells than the outbred controls. Effective utilization of this rabbit model could lead to a new tuberculosis diagnostic as well as to the elucidation of important correlates of protective immunity.

Human papillomavirus infections result in more than 250,000 deaths from cervical cancer in women worldwide. Hu et al. (2007) established a rabbit transgenic model expressing the human major histocompatibility complex (MHC-I) gene (HLA-A2.1). These transgenic rabbits expressed the HLA protein at a high level and HLA-A2.1 restricted rabbit CD8 cells were induced in these animals. Southern blot analysis demonstrated that the HLA-A2.1 gene was integrated into the rabbit genome and similar expression patterns of HLA-A2.1 and rabbit MHC class-I was observed in the three lines of transgenic rabbits. They demonstrated that HLA-A2.1 transgenic rabbits showed a susceptibility to cottontail rabbit papillomavirus infection akin to that of normal domestic rabbits. They also reported that a human papillomavirus type 16 E7 epitope can be engineered to be introduced into the cottontail rabbit papillomavirus E7 gene of the rabbit papillomavirus genome. This hybrid genome retained the ability to initiate paplillomas. The cottontail rabbit papillomavirus/HLA-A2.1 rabbit model has the potential to be used to screen HLA-A2.1-restricted immunogenic epitopes from human papillomaviruses in the context of in vivo papillomavirus infection. These studies suggested that rabbit is an excellent model to assess both natural and induced immunity to papillomavirus infections and that the transgenic rabbits may have utility for assessment of immunity to other human pathogens that are permissive in rabbits.

Rother reported the existence of a mutant rabbit which was deficient in the sixth component of complement (Rother et al. 1966). Current studies based on the use of the 6 complement-deficient rabbits suggested that this component is involved in the activity of the immune system, the activation of the inflammatory response and the hemolytic activity. Chartrand et al. (1979) demonstrated that delayed rejection was observed in the puppy hearts engrafted to C6-deficient rabbits. Schmiedt et al. (1998) suggested that C6-deficient rabbits delayed the development of atherosclerosis by cholesterol feeding due to the weak inflammatory responses of arterial cells. Therefore, C6-deficient rabbits may contribute to study human diseases related to the immune system and the inflammatory responses.

7.4.4 Rabbit Models for Human Articular Lesions and Therapeutics

Patients with articular cartilage lesions caused by injury or degenerative joint diseases become increased recently and these defects do not repair spontaneously. Studies using rabbits have been contributed to tentatively develop therapeutics against the diseases. Ikeda et al. (2009) showed that rabbits are useful to examine the effect on porosity and of the mechanical properties of a synthetic polymer (DL-lactide-coglycolide) scaffold on repair of osteochondral defects. They treated rabbits suffering from osteochondral defects in the femoral condyle with three types of scaffolds. Their study suggested that higher porosity allowing bone marrow cells to migrate to the scaffold is important in repairing osteochondral defects. Nakayama et al. (2009) performed a mechanical analysis of the effects of fibroblast growth factor-2 (FGF-2) on autologous osteochondral transplantation in an artificial rabbit model. They induced a full-thickness cartilage defect in the right femoral condyle and treated with osteochondral transplantation using an osteochondral plug taken from the left femoral condyle. Autologous osteochondral grafts transplanted with gelatin hydrogel containing FGF-2 acquired adequate stiffness at early postoperative phase. In addition, Ishida et al. (2007) demonstrated that platelet-rich plasma enhances the healing of meniscal defects in rabbits. These studies demonstrate that rabbits are useful for studies to develop therapeutics about human articular lesions.

7.4.5 Rabbit Models for Vascular Surgery

Rabbits are also useful for studies to develop technique for vascular and respiratory surgery. Kawanishi et al. (2007) showed that the prevention of back-bleeding from intercostal arteries and lumbar arteries during thoracoabdominal aortic surgery was considered to reduce spinal ischemic injury. They examined the effects of back-bleeding in spinal cord by comparing rabbits without back-bleeding from

the lumbar arteries by draining from the aorta during aortic clamping with rabbits in which back-bleeding was not drained. Forty-eight hours later, the number of TUNEL-positive cells in rabbits draining back-bleeding was significantly smaller than those in rabbits with back-bleeding. Hasegawa et al. (2007) implanted autologous fibrin-coated vascular prostheses and/or xenologous fibrin-coated vascular prostheses in the bilateral carotid arteries of JW rabbits. As a result, autologous fibrin coating in thrombin-free fibrin-coated vascular prostheses improved antithrombogenecity. Their study suggested that autologous fibrin coating in thrombin-free fibrin-coated vascular prostheses have a potential for clinical use in hybrid small-caliber vascular grafts.

7.4.6 Rabbit Models for Tumor Study

Several transplantable rabbit tumors have been reported and VX2 tumor has been used in some studies. The VX2 carcinoma arose as the result of spontaneous transformation of a virus-induced skin papilloma in a domestic rabbit (Kidd and Rous 1940) and is a type of dermatological squamous cancer induced by the Shope virus. In general, the VX-2 tumor had a high malignant potential, with capacity for rapid reproduction, infiltration and metastasis. VX2 tumors have been transplanted into lung, liver, and other organs in rabbits. These rabbit VX2 tumors have been studied for establishing therapeutics and diagnostics. Virmani et al. (2008) demonstrated that hypoxia caused by transcatheter arterial embolization of VX2 liver tumors activates the hypoxia-inducible factor-1 alpha, a transcription factor that in turn regulates other pro-angiogenic factors. Jiang et al. (2008) reported that the hemodynamic changes in the liver caused by rabbit VX2 liver tumor can be detectable after tumor inoculation and that functional CT can evaluate the physiological characteristics of early angiogenesis. In addition, Ohira et al. (2008) demonstrated that FDG-PET was useful for monitoring the early effects of radiofrequency ablation in VX2 rabbit tumors implanted into the back muscles. These studies have demonstrated that rabbits are also useful for studies of tumor.

7.5 Conclusions

Genetically modified mice is playing an essential role in the clarification of the expression and functions of individual gene. However, to translate or extrapolate the results of animal studies to humans, it is necessary that key gene expression and function are equivalent to human rather than the outward features or phenotype. For example, to study human hypercholesterolemia, not only the hyperlipidemia itself, the characteristics of the lipoprotein profiles and enzymes in the lipoprotein metabolism of animal models is vitally important for translational researches. In addition, histopathological and/or immunohistochemical features similar to humans are

also important. Several rabbit models for some human diseases described in this chapter are useful in translational researches. Applying these animal models in translational researches will contribute to elucidation of the mechanism of human diseases and development of novel compounds, therapeutics, or diagnostic instruments containing lesion imaging techniques.

Acknowledgements This work was supported partly by a research grant from the Health and Labor Ministry of Japan and unrestricted research grants from Sankyo Co. Ltd., Japan.

References

Anitschkow NN, Chalatow S (Translated by Pelias MZ). (1983) On experimental cholesterin steatosis and its significance in the origin of some pathological processes. Arteriosclerosis 3: 178–182. (The original article: Ueber experimentelle cholesterinsteatose und ihre bedeutung für die entstehung einiger pathologischer prozesse. Zentralbl Allg Pathol Pathol Anat 1913; 24: 1–9.)

Ardern HA, Benson GM, Suckling KE, Caslake MJ, Shepherd J, Packard CJ. (1999) Apolopoprotein B overproduction by the perfused liver of the St. Thomas' mixed hyperlipidemic (SMHL) rabbit. J Lipid Res 40: 2234–2243.

Brunner M, Peng X, Liu GX, Ren Z, Ziv O, Choi B, Mathur R, Hajjiri M, Odening KE, Steinberg E, Folco EJ, Pringa E, Centracchio J, Macharzina RR, Donahay T, Schofield L, Rana N, Kirk M, Mitchell GF, Poppas A, Zehender M, Koren G. (2008) Mechanisms of cardiac arrhythmias and sudden death in transgenic rabbits with long QT syndrome. J Clin Invest 118: 2246–2259.

Chartrand C, O'Regan S, Robitaille P, Pino-Blonde M. (1979) Delayed rejection of cardiac xenografts in C6-defficient rabbits. Immunology 38: 245–248.

Cybulsky MI, Gimbrone MA. (1991) Endothelial expression of a mononuclear leukocyte adhesion molecule during atherogenesis. Science 251: 788–791.

De Roos B, Caslake MJ, Ardern HA, Benson GM, Suckling KE, Packard CJ. (2001) Insulin resistance in the St. Thomas' mixed hyperlipidemic (SMHL) rabbit, a model for familial combined hyperlipidemia. Atherosclerosis156: 249–254.

De Roos B, Caslake MJ, Milliner K, Benson GM, Suckling KE, Packard CJ. (2005) Characterisation of the lipoprotein structure in the St. Thomas' mixed hyperlipidemic (SMHL) rabbit. Atherosclerosis 181: 63–68.

Fan J, Watanabe T. (2003) Transgenic rabbits as therapeutic protein bioreactors and human disease models. Pharmacol Ther 99: 261–282.

Fleet JC, Clinton SK, Salomon RN, Loppnow H, Libby P. (1992) Atherogenic diets enhance endoxin-stimulated interleukin-1 and tumor necrosis factor gene expression in rabbit aorta. J Nutr 122: 294–305.

Galis ZS, Sukhova GK, Kränzhofer R, Clark S, Libby P. (1995) Macrophage foam cells from experimental atheroma constitutively produce matrix-degradation proteins. Proc Natl Acad Sci USA 92: 402–406.

Garibaldi BA, Goad MEP. (1998) Lipid keratopathy in the Watanabe (WHHL) rabbit. Vet Pathol 25: 173–174.

Goldstein JL, Kita T, Brown MS. (1983) Defective lipoprotein receptors and atherosclerosis: lessons from an animal counterpart of familial hypercholesterolemia. N Engl J Med 309: 288–296.

Hasegawa T, Okada K, Takano Y, Hiraishi Y, Okita Y. (2007) Autologous fibrin-coated small-caliber vascular prostheses improve antithrombogenecity by reducing immunologic response. J Thorac Cardiovasc Surg 133: 1268–1276.

Hoshiba Y, Hatakeyama K, Tanabe T, Asada Y, Goto S. (2006) Co-localization of von Willebrand factor with platelet thrombi, tissue factor and platelets with fibrin, and consistent presence of inflammatory cells in coronary thrombi obtained by an aspiration device from patients with acute myocardial infarction. J Thromb Haemost 3: 1140–1120.

Hu J, Peng X, Budgeon LR, Cladel NM, Balogh KK, Christensen ND. (2007) Establishment of a cottontail rabbit papillomavirus/HLA-A2.1 transgenic rabbit model. J Virol 81: 7171–7177.

Ikeda R, Fujioka H, Nagura I, Kokubu T, Toyokawa N, Inui A, Makino T, Kaneko H, Doita M, Kurosaka M. (2009) The effects of porosity and mechanical property of a synthetic polymer scaffold on repair of osteochondral defects. Int Orthop (in press).

Ishida K, Kuroda R, Miwa M, Tabata Y, Hokugo A, Kawamoto T, Sasaki K, Doita M, Kurosaka M. (2007) The regenerative effects of platelet-rich plasma on meniscal cells in vitro and its in vivo application with biodegradable gelatin hydrogel. Tissue Eng 13: 1103–1112.

Ishino S, Mukai T, Kume N, Asano D, Ogawa M, Kuge Y, Minami M, Kita T, Shiomi M, Saji H. (2007) Lectin-like oxidized LDL receptor-1 (LOX-1) expression is associated with atherosclerotic plaque instability-analysis in hypercholesterolemic rabbits. Atherosclerosis 195: 48–56.

Ito T, Yamada S, Shiomi M. (2004) Progression of coronary atherosclerosis relates to the onset of myocardial infarction in an animal model of spontaneous myocardial infarction (WHHLMI rabbits). Exp Anim 53: 339–334.

Iwata A, Miura S, Imaizumi B, Saku K. (2007) Measurement of atherosclerotic plaque volume in hyperlipidemic rabbit aorta by intravascular ultrasound. J Cardiol 50: 229–234.

Jiang HJ, Zhang ZR, Shen BZ, Wan Y, Guo H, Shu SJ. (2008) Functional CT for assessment of early vascular physiology in liver tumors. Hepatobiliary Pancreat Dis Int 7: 497–502.

Kawai T, Ito T, Ohwada K, Mera Y, Matsushita M, Tomoike H. (2006) Hereditary postprandial hypertriglyceridemic rabbit exhibits insulin resistance and central obesity: a novel model of metabolic syndrome. Arterioscler Thromb Vasc Biol 26: 2752–2757.

Kawanishi Y, Okada K, Tanata H, Yamashota T, Nakagiri K, Okita Y. (2007) The adverse effect of back-bleeding from lumber arteries on spinal cord pathophysiology in a rabbit model. J Thorac Cardiovasc Surg 133: 1553–1558.

Kidd JG, Rous P. (1940) A transplantable rabbit carcinoma originating in a virus-induced papilloma and containing the virus in masked or altered form. J Exp Med 71: 813–838.

Kita T, Brown MS, Watanabe Y, Goldstein JL. (1981) Deficiency of low density lipoprotein receptors in liver and adrenal gland of the WHHL rabbit, an animal model of familial hypercholesterolemia. Proc Natl Acad Sci USA 78: 2268–2272.

Kozarsky KF, Bonen DK, Giannoni F, Funahashi T, Wilson JM, Davivson NO. (1996) Hepatic expression of the catalytic subunit of the apolipoprotein B mRNA editing enzyme (apobec-1) ameliorates hypercholesterolemia in LDL receptor-deficient rabbits. Hum Gene Ther 7: 973–977.

La Ville A, Turner PR, Pititlo RM, Martini S, Marenah CB, Rowles PM, Morris G. (1987) Thomson GA, Woolf N, Lewis B. Hereditary hyperlipidemia in the rabbit due to overproduction of lipoproteins. I. Biochemical studies. Arteriosclerosis 7: 105–112

Manabe YC, Kesavan AK, Lopez-Molina J, Hatem CL, Brooks M, Fujiwara R, Hochstein K, Pitt MLM, Tufariello J, Chan J, McMurray DN, Bishai WR, Dannenberg AM, Mendez S. (2008) The aerosol rabbit model of TB latency, reactivation and immune reconstitution inflammatory syndrome. Tuberculosis 88: 187–196.

Mendez S, Hatem CL, Kesavan AK, Lopez-Molina J, Pitt ML, Dannenberg AM Jr, Manabe YC. (2008) Susceptibility to tuberculosis: composition of tuberculous granulomas in Thorbecke and outbred New Zealand white rabbits. Vet Immunol Immunopathol 122: 167–174.

Meding J, Urich M, Licha K, Reinhardt M, Misselwitz B, Fayad ZA, Weinmann HJ. (2007) Magnetic resonance imaging of atherosclerosis by targeting extracellular matrix deposition with Gadofluorine M. Contrast Media Mol Imag 2: 120–129.

Naghavi M, Libby P, Falk E, Casscells SW, Litovsky S, Rumberger J, Badimon JJ, Stefanadis C, Moreno P, Pasterkamp G, Fayad Z, Stone PH, Waxman S, Raggi P, Madjid M, Zarrabi A, Burke A, Yuan C, Fitzgerald PJ, Siscovick DS, de Korte CL, Aikawa M, Airaksinen KEJ, Assmann G, Becker CR, Chesebro JH, Farb A, Galis ZS, Jackson C, Jang I, Koenig W,

Lodder RA, March K, Demirovic J, Navab M, Priori SG, Rekhter MD, Bahr R, Grundy SM, Mehran R, Colombo A, Boerwinkle E, Ballantyne C, Insull W Jr, Schwartz RS, Vogel R, Serruys PW, Hansson GK, Faxon DP, Kaul S, Drexler H, Greenland P, Muller JE, Virmani R, Ridker PM, Zipes DP, Shah PK, and Willerson JT. (2003) From vulnerable plaques to vulnerable patients, a call for new definitions and risk assessment strategies: Part I. Circulation 108: 1664–1672.

Nakayama J, Fujioka H, Nagura I, Kokubu T, Makino T, Kuroda R, Tabata Y, Kurosaka M. (2009) The effect of fibroblast growth factor-2 on autologous osteochondral transplantation. Int Orthop 33: 275–280.

Odening KE, Hyder O, Chaves L, Schofield L, Brunner M, Kirk M, Zehender M, Peng X, Koren G. (2008) Pharmacogenomics of anesthetic drugs in transgenic LQT1 and LQT2 rabbits reveal genotype-specific differential effects on cardiac repolarization. Am J physiol Heart Circ Physiol 295: H2264–H2272.

Ogawa M, Magata Y, Kato T, Hatano K, Ishino S, Mukai T, Shiomi M, Ito K, Saji H. (2006) Application of 18F-FDG PET for monitoring the therapeutic effect of antiinflammatory drugs on stabilization of vulnerable atherosclerotic plaques. J Nucl Med 47: 1845–1850.

Ohira T, Okuma T, Matsuoka T, Wada Y, Nakamura K, Watanabe Y, Inoue Y. (2009) FDG-MicroPET and diffusion-weighted MR image evaluation of early changes after radiofrequency ablation in implanted VX2 tumors in rabbits. Cardiovasc Intervent Radiol 32: 114–120.

Rosenfeld ME, Tsukada T, Gown AM, Ross R. (1987) Fatty streak initiation in Watanabe heritable hyperlipidemic and comparably hypercholesterolemic fat-fed rabbits. Arteriosclerosis 7: 9–23.

Rosenfeld ME, Ylä-herttuala S, Lipton BA, Ord VA, Witztum JL, Steinberg D. (1992) Macrophage colony-stimulating factor mRNA and protein in atherosclerotic lesions of rabbits and humans. Am J Pathol 140: 291–300.

Rother K, Rother U, Muller-Eberhard HJ, Nilsson UR. (1966) Defficiency of the sixth component of complement in rabbits with an inherited complement defect. J Exp Med 124: 773–785.

Schmiedt W, Kinscherf R, Deigner HP, Kamencic H, Nauen O, Kilo J, Oelert H, Metz J, Bhakdi S. (1998) Complement C6 deficiency protects against diet-induced atherosclerosis in rabbits. Arterioscler Throm Vasc Biol 18: 1790–1795.

Shiomi M, Fan J. (2008) Unstable coronary plaques and cardiac events in myocardial infarction-prone Watanabe heritable hyperlipidemic (WHHLMI) rabbits: questions and quandaries. Curr Opin Lipidol 19: 631–636.

Shiomi M, Ito T. (1999a) Effect of cerivastatin sodium, a new inhibitor of HMG-CoA reductase, on plasma lipid levels, progression of atherosclerosis, and the lesional composition in the plaques of WHHL rabbits. Br J Pharmacol 126: 961–968.

Shiomi M, Ito T, Tsukada T, Tsujita Y, Horikoshi H. (1999b) Combination treatment with troglitazone, an insulin action enhancer, and pravastatin, an inhibitor of HMG-CoA reductase, shows synergistic effect on atherosclerosis of WHHL rabbits. Atherosclerosis 42: 345–353.

Shiomi M, Ito T, Tsukada T, Yata T, Ueda M. (1994) Cell compositions of coronary and aortic atherosclerotic lesions differ; An immunohistochemical study. Arterioscler Thromb 14: 931–937.

Shiomi M, Ito T, Tsukada T, Yata T, Watanabe Y, Tsujita Y, Fukami M, Fukushige J, Hosokawa T, Tamura A. (1995) Reduction of serum cholesterol levels alters lesional composition of atherosclerotic plaques: effect of pravastatin sodium on atherosclerosis in mature WHHL rabbits. Arterioscler Thromb Vasc Biol 15: 1938–1944.

Shiomi M, Ito T, Yamada S, Kawashima S, Fan J. (2003) Development of an animal model for spontaneous myocardial infarction (WHHLMI Rabbit). Arterioscler Thromb Vasc Biol 23: 1239–1244.

Shiomi M, Yamada S, Ito T. (2005) Atheroma stabilizing effects of simvastatin due to depression of macrophages or lipid accumulation in the atheromatous plaques of coronary atherosclerosis-prone WHHL rabbits. Atherosclerosis 178: 287–294.

Son YC, Zilversmit DB. (1986) Increased lipid transfer activities in hyperlipidemic rabbit plasma. Arteriosclerosis 6: 345–351.

Sieen H, Lima JA, Chatterjee S, Kolmakova A, Gao F, Rodrigues ER, Stuber M. (2007) High-resolution three-dimensional aortic magnetic resonance angiography and quantitative vessel wall characterization of different atherosclerotic stages in a rabbit model. Invest Radiol 42: 614–621.

Tanzawa K, Shimada Y, Kuroda M, Tsujita Y, Arai M, Watanabe Y. (1980) WHHL-rabbit; a low density lipoprotein receptor-deficient animal model for familial hypercholesterolemia. FEBS Lett 118: 81–84.

Tsujita Y, Kuroda M, Shimada Y, Tanzawa K, Arai M, Kaneko I, Tanaka M, Masuda H, Tarumi C, Watanabe Y, Fujii S. (1986) CS-514, a competitive inhibitor of 3-hydroxy-3-methylglutaryl coenzyme A reductase: tissue-selective inhibition of sterol synthesis and hypolipidemic effect on various animal species. Biochim Biophys Acta 877: 50–60.

Virmani S, Rhee TK, Ryu RK, Sato KT, Lewandowski RJ, Mulcahy MF, Kulik LM, Szolc-Kowalska B, Woloschak GE, Yang GY, Salem R, Larsin AC, Omary RA. (2008) Comparison of hypoxia-inducible factor-1alpha expression before and after transcatheter arterial embolisation in rabbit VX2 liver tumors. J Vasc Interv Radiolo 19: 1483–1489.

Watanabe Y. (1980) Serial inbreeding of rabbits with hereditary hyperlipidemia (WHHL-rabbit). Atherosclerosis 36: 261–268.

Watanabe Y, Ito T, Saeki M, Kuroda M, Tanzawa K, Mochizuki M, Tsujita Y, Arai M. (1981) Hypolipidemic effects of CS-500 (ML-236B) in WHHL-rabbit, a heritable animal model for hyperlipidemia. Atherosclerosis 38: 27–31.

Watanabe Y, Ito T, Shiomi M. (1985) The effect of selective breeding on the development of coronary atherosclerosis. Atherosclerosis 56: 71–79.

Watanabe Y, Ito T, Shiomi M, Tsujita Y, Kuroda M, Arai M, Fukami M, Tamura A. (1988) Preventive effect of pravastatin sodium, a potent inhibitor of 3-hydroxy-3-methylglutaryl coenzyme A reductase, on coronary atherosclerosis and xanthoma in WHHL rabbits. Biochim Biophys Acta 960: 294–302.

Yamamoto T, Bishop RW, Brown MS, Goldstein JL, Russell DW. (1986) Deletion in cysteine-rich region of LDL receptor impedes transport to cell surface in WHHL rabbit. Science 232: 1230–1237.

Yamashita A, Furukoli E, Marutsuka K, Hatakeyama K, Yamamoto H, Tamura S, Ikeda Y, Sumiyoshi A, Asada Y. (2004) Increased vascular wall thrombogenicity combined with reduced blood flow promotes occlusive thrombus formation in rabbit femoral artery. Arterioscler Thromb Vasc Biol 24: 2420–2424.

Ylä-Herttuala S, Lipton BA, Rosenfeld ME, Särkioja T, Yoshimura T, Leonard EJ, Witztum JL, Steiberg D. (1991) Expression of monocyte chemoattractant protein 1 in macrophage-rich areas of human and rabbit atherosclerotic lesions. Proc Natl Acd Sci USA 88: 5252–5256.

Zhang B, Saku K, Hirata K, Liu R. (1991) Tateishi K, Yamamoto K, Arakawa K. Insulin resistance observed in WHHL rabbits. Atherosclerosis 91: 277–278.

Bioorganic & Medicinal Chemistry 17 (2009) 2069–2076

Contents lists available at ScienceDirect

Bioorganic & Medicinal Chemistry

journal homepage: www.elsevier.com/locate/bmc

^{18}F-labeled flavones for in vivo imaging of b-amyloid plaques in Alzheimer's brains

Masahiro Ono [a,b,*], Rumi Watanabe [a], Hidekazu Kawashima [c], Tomoki Kawai [b], Hiroyuki Watanabe [a], Mamoru Haratake [a], Hideo Saji [b], Morio Nakayama [a,*]

[a] Graduate School of Biomedical Sciences, Nagasaki University, 1-14 Bunkyo-machi, Nagasaki 852-8521, Japan
[b] Graduate School of Pharmaceutical Sciences, Kyoto University, 46-29 Yoshida Shimoadachi-cho, Sakyo-ku, Kyoto 606-8501, Japan
[c] Graduate School of Medicine, Kyoto University, Shogoin Kawahara-cho, Sakyo-ku, Kyoto 606-8507, Japan

article info

Article history:
Received 10 December 2008
Revised 6 January 2009
Accepted 7 January 2009
Available online 20 January 2009

Keywords:
Alzheimer's disease
β-Amyloid plaque
PET
Flavone

abstract

In vivo imaging of β-amyloid (Aβ) aggregates in the brain may lead to early detection of Alzheimer's disease (AD) and monitoring of the progression and effectiveness of treatment. The purpose of this study was to develop novel ^{18}F-labeled amyloid-imaging probes based on flavones as a core structure. Fluoropegylated (FPEG) flavone derivatives were designed and synthesized. The affinity of the derivatives for Aβ aggregates varied from 5 to 321 nM. In brain sections of AD model mice, FPEG flavones with the dimethylamino group intensely stained β-amyloid plaques. In biodistrubution experiments using normal mice, they displayed high uptake in the brain ranging from 2.9 to 4.2%ID/g at 2 min postinjection. The radioactivity washed out from the brain rapidly (1.3–2.0%ID/g at 30 min), which is highly desirable for β-amyloid imaging agents. FPEG flavones may be potential PET imaging agents for β-amyloid plaques in Alzheimer's brains.

1. Introduction

Alzheimer's disease (AD) is a progressive neurodegenerative disorder characterized by cognitive decline, irreversible memory loss, disorientation, and language impairment. The presence of β-amyloid (Aβ) aggregates in the brain is generally accepted as a hallmark of AD.[1,2] Since the only definitive diagnosis of AD is by pathological examination of postmortem staining of affected brain tissues, the development of techniques which enable one to image β-amyloid plaques in vivo has been strongly desired.[3–5]

Recent success in developing radiolabeled agents targeting Aβ aggregates has provided a window of opportunity to improve the diagnosis of AD. Preliminary reports of positron emission tomography (PET) imaging suggested that [^{11}C]4-N-methylamino-4$^{\bar{1}}$-hydroxystilbene (SB-13),[6,7] [^{11}C] 2-(4$^{\bar{1}}$-(methylaminophenyl)-6-hydroxy benzothiazole (PIB),[8,9] and [^{11}C]2-(2-[2-dimethylaminothiazol-5-yl]ethenyl)-6-(2-[fluoro]ethoxy)benzoxazole (BF-227)[10] showed differential uptake and retention in the brain of AD patients as compared to controls. But ^{11}C is a positron-emitting isotope with a short $t_{1/2}$ (20 min), which limits its clinical application. Recent efforts have focused on the development of comparable agents labeled with a longer half-life isotope, ^{18}F ($t_{1/2}$: 110 min). Preliminary studies with [^{18}F]-2-(1-(2-(N-(2-fluoroethyl)-N-methylamino)-naphthalen-6-yl)ethylidene)malononitrile ([^{18}F]FDDNP)[11,12] showed differential uptake and retention in the brain of AD patients for the first time. More recently, a stilbene derivative, [^{18}F]BAY94-9172, has been shown to be useful for the imaging of β-amyloid plaques in living human brain tissue in clinical trials.[13]

To search for more candidates for ^{18}F-labeled β-amyloid imaging agents for PET, we planned to evaluate a new series of flavone derivatives previously reported as useful for imaging β-amyloid by single photon emission computed tomography (SPECT).[14] The derivatives showed good affinity for Aβ aggregates in vitro in binding experiments using synthetic Aβ aggregates and neuropathological staining of AD brain sections, suggesting these classes of radioiodinated flavones to be potential imaging agents.

Recently, Kung et al. exploited a novel approach by using fluoro-pegylation (FPEG) of the core structure for ^{18}F labeling of derivatives.[15] Since this approach offers a simple and easy way to incorporate ^{18}F into the target without an appreciable increase in lipophilicity, we planned to apply it to the labeling of flavone derivatives. In addition to the structural characteristics of flavone as the pharmacophore, it has been shown that electron-donating groups such as amino, methylamino, dimethylamino, methoxy, or hydroxy groups play a critical role in the binding of Aβ aggregates.[6,8,16,17] With these considerations, we designed 12 fluorinated flavones with a fluorine or FPEGylation at position 4 and an electron-donating group at position 4$^{\bar{1}}$ (Fig. 1).

* Corresponding authors. Tel.: +81 75 753 4608; fax: +81 75 753 4568 (M.O.); tel./fax: +81 95 819 2441 (M.N.).
E-mail addresses: ono@pharm.kyoto-u.ac.jp, mono@net.nagasaki-u.ac.jp (M. Ono) morio@nagasaki-u.ac.jp (M. Nakayama).

0968-0896/$ - see front matter
doi:10.1016/j.bmc.2009.01.025

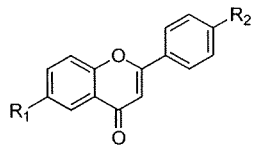

Compound	R_1	R_2
8a	FCH_2CH_2O	$N(CH_3)_2$
8b	$F(CH_2CH_2O)_2$	$N(CH_3)_2$
8c	$F(CH_2CH_2O)_3$	$N(CH_3)_2$
12	FCH_2CH_2O	NH_2
13	FCH_2CH_2O	$NHCH_3$
15b	$F(CH_2CH_2O)_2$	NH_2
15c	$F(CH_2CH_2O)_3$	NH_2
17b	$F(CH_2CH_2O)_2$	$NHCH_3$
17c	$F(CH_2CH_2O)_3$	$NHCH_3$
21	F	NH_2
22	F	$NHCH_3$
23	F	$N(CH_3)_2$

Figure 1. Chemical structure of FPEG-flavone derivatives.

We report here the in vitro and in vivo evaluation of a new series of flavone derivatives as agents for imaging β-amyloid with PET.

2. Experimental

All reagents were commercial products and used without further purification unless otherwise indicated. ^{1}H NMR spectra were obtained on a Varian Gemini 300 spectrometer with TMS as an internal standard. Coupling constants are reported in hertz. Multiplicity is defined by s (singlet), d (doublet), t (triplet), br (broad), and m (multiplet). Mass spectra were obtained on a JEOL IMS-DX instrument.

2.1. Chemistry

2.1.1. 4-Nitrobenzoic acid 2-acetyl-4-methoxyphenyl ester (1)

To a stirring solution of 4-nitrobenzoyl chloride (1.8 g, 10 mmol) in pyridine (20 mL) was added 2-hydroxy-5-methoxyacetophenone (1.6 g, 10 mmol). The reaction mixture was stirred at room temperature for 3 h, and poured into a 1 N aqueous HCl/ice solution with vigorous stirring. The precipitate that formed was filtered and washed with water to yield acetophenone 1 (2.9 g, 90.4% yield). ^{1}H NMR (300 MHz, $CDCl_3$) δ: 2.54 (s, 3H), 3.89 (s, 3H), 7.15–7.16 (m, 2H), 7.38 (d, J = 2.0 Hz, 1H), 8.37 (s, 4H).

2.1.2. 1-(5-Methoxy-2-hydroxyphenyl)-3-(4-nitrophenyl)propane-1,3-dione (2)

A solution of acetophenone 1 (2.9 g, 9.0 mmol) and pyridine (50 mL) was heated to 50 C, and to it was added pulverized potassium hydroxide (2.5 g, 45.2 mmol). The reaction mixture was stirred for 90 min, and when it had cooled, 30 mL of 10% aqueous acetic acid solution was added. The yellow precipitate that formed was filtered to yield 2 (2.5 g, 88.1% yield). ^{1}H NMR (300 MHz, $CDCl_3$) δ: 3.85 (s, 3H), 6.84 (s, 1H), 6.99 (d, J = 6.9 Hz, 1H), 7.15–7.18 (m, 1H), 7.22 (d, J = 2.2 Hz, 1H), 8.10 (d, J = 6.6 Hz, 2H), 8.35 (d, J = 6.6 Hz, 2H), 11.5 (s, 1H).

2.1.3. 6-Methoxy-4^1-nitroflavone (3)

A mixture of the diketone 2 (2.5 g, 8.0 mmol), concentrated sulfuric acid (2 mL), and glacial acetic acid (40 mL) was heated at 100 C for 2 h and cooled to room temperature. The mixture was poured onto crushed ice, and the resulting precipitate was filtered to yield 3 (1.5 g, 63.5%). ^{1}H NMR (300 MHz, $CDCl_3$) δ: 3.93 (s, 3H), 6.92 (s, 1H), 7.31–7.37 (m, 1H), 7.54–7.61 (m, 2H), 8.11 (d, J = 9.3 Hz, 2H), 8.39 (d, J = 9.3 Hz, 2H).

2.1.4. 6-Methoxy-4^1-aminoflavone (4)

A mixture of 3 (3.0 g, 10.2 mmol), $SnCl_2$ (7.6 g, 39.8 mmol), and EtOH (30 mL) was stirred under reflux for 40 min. After the mixture had cooled to room temperature, 1 M NaOH (50 mL) was added until the mixture became alkaline. After extraction with ethyl acetate, the combined organic layers were washed with brine, dried over Na_2SO_4, and filtered. The solvent was removed, and the residue was purified by silica gel chromatography (hexane/ethyl acetate = 1:2) to give 1.3 g of 4 (65.3% yield). ^{1}H NMR (300 MHz, $CDCl_3$) δ: 3.91 (s, 3H), 4.11 (s, broad, 2H), 6.69 (s, 1H), 6.75 (d, J = 6.6 Hz, 2H), 7.24–7.27 (m, 1H), 7.47 (d, J = 6.6 Hz, 1H), 7.59 (d, J = 2.2 Hz, 1H), 7.75 (d, J = 6.6 Hz, 2H).

2.1.5. 6-Methoxy-4^1-dimethylaminoflavone (5)

To a mixture of 4 (401 mg, 1.5 mmol) and paraformaldehyde (450 mg, 15 mmol) in AcOH (10 mL) was added $NaCNBH_3$ (471 mg, 7.5 mmol) in one portion at room temperature. The resulting mixture was stirred at room temperature for 1.5 h, and the addition of 1 M NaOH was followed by extraction with CH_3Cl. The organic phase was dried over Na_2SO_4. The solvent was removed, and the residue was purified by silica gel chromatography ($CHCl_3$/MeOH = 20:1) to give 371 mg of 5 (83.7% yield). ^{1}H NMR (300 MHz, $CDCl_3$) δ: 3.07 (s, 6H), 3.91 (s, 3H), 6.70 (s, 1H), 6.75 (d, J = 9.0 Hz, 2H), 7.24–7.26 (m, 1H), 7.47 (d, J = 9.0 Hz, 1H), 7.59 (d, J = 2.2 Hz, 1H), 7.81 (d, J = 9.0 Hz, 2H).

2.1.6. 6-Hydroxy-4^1-dimethylaminoflavone (6)

To a solution of 5 (371 mg, 1.5 mmol) in CH_2Cl_2 (10 mL) at 10 C was added BBr_3 (7.5 mL, 1 M solution in CH_2Cl_2) dropwise in an ice bath. The mixture was allowed to warm to room temperature and was stirred for 12 h. Water was added while the reaction mixture was cooled in an ice bath to keep the reaction temperature at 0 C. After extraction with CH_2Cl_2, the combined organic phase was dried over Na_2SO_4. The filtrate was concentrated and the residue was purified by silica gel chromatography ($CHCl_3$/MeOH = 20:1) to give 303 mg of 6 (71.8% yield). ^{1}H NMR (300 MHz, $CDCl_3$) δ: 3.05 (s, 6H), 6.74 (d, J = 9.3 Hz, 2H), 7.26 (d, J = 3.0 Hz, 1H), 7.45 (d, J = 9.0 Hz, 1H), 7.58 (d, J = 3.0 Hz, 1H), 7.77 (d, J = 9.0 Hz, 2H).

2.1.7. 6-Hydroxyethoxy-4^1-dimethylaminoflavone (7a)

To a solution of 6 (85 mg, 0.30 mmol) and ethylene chlorohydrin (100 μL, 1.50 mmol) in DMSO (3 mL) was added anhydrous K_2CO_3 (41 mg, 0.90 mmol). The reaction mixture was stirred at 120 C for 48 h, then poured into water. After extraction with chloroform, the organic layers were combined and dried over Na_2SO_4. Evaporation of the solvent afforded a residue, which was purified by silica gel chromatography ($CHCl_3$/MeOH = 33:1) to give 30 mg of 7a (30.5%). ^{1}H NMR (300 MHz, $CDCl_3$) δ: 3.06 (s, 6H), 3.98–4.05 (m, 2H), 4.17–4.23 (m, 2H), 6.69 (s, 1H), 6.76 (d, J = 9.3 Hz, 2H), 7.28 (d, J = 3.0 Hz, 1H), 7.47 (d, J = 9.0 Hz, 1H), 7.60 (d, J = 3.0 Hz, 1H), 7.80 (d, J = 9.0 Hz, 2H).

2.1.8. 6-(2-(2-Hydroxy-ethoxy)-ethoxy)-4^1-dimethylaminoflavone (7b)

To a solution of 6 (82 mg, 0.29 mmol) and ethylene glycol mono-2-chloroethyl ether (37 μL, 0.35 mmol) in DMF (3 mL) was added anhydrous K_2CO_3 (120 mg, 0.87 mmol). The reaction mixture was stirred at 120 C for 11 h, then poured into water. After extraction with chloroform, the organic layers were combined and dried over Na_2SO_4. Evaporation of the solvent afforded a residue, which was purified by silica gel chromatography (hexane/ethyl acetate = 10:1) to give 107 mg of 7b (99.3%). ^{1}H NMR (300 MHz, $CDCl_3$) δ: 3.07 (s, 6H), 3.69 (t, J = 5.1 Hz, 2H), 3.79 (s, 2H), 3.91 (t, J = 4.5 Hz, 2H), 4.26 (t, J = 4.5 Hz, 2H), 6.69 (s, 1H), 6.75 (d, J = 9.0 Hz, 2H), 7.27–7.30 (m, 1H), 7.47 (d, J = 9.0 Hz, 1H), 7.64 (d, J = 2.2, 1H), 7.81 (d, J = 9.0 Hz, 2H).

2.1.9. 6-(2-(2-(2-Hydroxy-ethoxy)-ethoxy)ethoxy)-4^{I}-dimethylaminoflavone (7c)

To a solution of 6 (100 mg, 0.36 mmol) and 2-[2-(2-chloroethoxy)ethoxy]ethanol (62 μL, 0.43 mmol) in DMF (3 mL) was added anhydrous K_2CO_3 (148 mg, 1.07 mmol). The reaction mixture was stirred at 120 C for 17 h, then poured into water. After extraction with chloroform, the organic layers were combined and dried over Na_2SO_4. Evaporation of the solvent afforded a residue, which was purified by preparative TLC ($CHCl_3$/MeOH = 20:1) to give 76 mg of 7c (51.1%). ^{1}H NMR (300 MHz, $CDCl_3$) δ: 3.07 (s, 6H), 3.62–3.76 (m, 8H), 3.91 (t, J = 4.5 Hz, 2H), 4.26 (t, J = 4.5 Hz, 2H), 6.69 (s, 1H), 6.77 (d, J = 9.3 Hz, 2H), 7.28–7.33 (m, 1H), 7.47 (d, J = 9.0 Hz, 1H), 7.60 (d, J = 2.2, 1H), 7.81 (d, J = 9.0 Hz, 2H).

2.1.10. 6-Fluoroethoxy-4^{I}-dimethylaminoflavone (8a)

To a solution of 7a (30 mg, 0.09 mmol) in ethylene glycol dimethyl ether (3 mL) was added dimethylamino sulfur trifluoride (DAST) (30 μL, 0.23 mmol) in a dry ice-acetone bath. The reaction mixture was stirred for 6 h at room temperature. The mixture was then poured into a saturated $NaHSO_3$ solution and after extraction with chloroform, the organic phase was separated, dried over Na_2SO_4, and filtered. The residue was purified by silica gel chromatography (hexane/ethyl acetate = 2:1) to give 16 mg of 8a (53.0%). ^{1}H NMR (300 MHz, $CDCl_3$) δ: 2.93 (s, 6H), 4.26–4.40 (m, 2H), 4.70–4.92 (m, 2H), 6.71 (s, 1H), 6.76 (d, J = 9.0 Hz, 2H), 7.29–7.35 (m, 1H), 7.50 (d, J = 9.0 Hz, 1H), 7.59 (d, J = 3.3 Hz, 1H), 7.82 (d, J = 9.3 Hz, 2H). EI-MS m/z 327 (M^+).

2.1.11. 6-(2-(2-Fluoro-ethoxy)-ethoxy)-4^{I}-dimethylaminoflavone (8b)

To a solution of 7b (29 mg, 0.08 mmol) in 1,2-dimethoxyethane (DME) (5 mL) was added DAST (21 μL, 0.16 mmol) in a dry ice-acetone bath. The reaction mixture was stirred for 1.5 h at room temperature. The mixture was then poured into a saturated $NaHSO_3$ solution and after extraction with chloroform, after the organic phase was separated, dried over Na_2SO_4, and filtered. The residue was purified by preparative TLC ($CHCl_3$/MeOH = 20:1) to give 15 mg of 8b (51.5%). ^{1}H NMR (300 MHz, $CDCl_3$) δ: 3.07 (s, 6H), 3.79 (t, J = 4.2 Hz, 1H), 3.89–3.96 (m, 3H), 4.26 (t, J = 4.8 Hz, 2H), 4.54 (t, J = 4.2 Hz), 4.69 (t, J = 4.2 Hz), 6.70 (s, 1H), 6.76 (d, J = 9.0 Hz, 2H), 7.27–7.33 (m, 1H), 7.49 (d, J = 9.3 Hz, 1H), 7.59 (d, J = 3.0, 1H), 7.81 (d, J = 9.0 Hz, 2H). EI-MS m/z 371 (M^+).

2.1.12. 6-(2-(2-(2-Fluoro-ethoxy)-ethoxy)ethoxy)-4^{I}-dimethylaminoflavone (8c)

To a solution of 7c (141 mg, 0.34 mmol) in DME (5 mL) was added DAST (90 μL, 0.68 mmol) in a dry ice-acetone bath. The reaction mixture was stirred for 1 h at room temperature. The mixture was then poured into saturated $NaHSO_3$ solution and extracted with chloroform. After the organic phase was separated, dried over Na_2SO_4 and filtered, the residue was purified by preparative TLC (hexane/ethyl acetate = 1:5) to give 21 mg of 8c (14.9%). ^{1}H NMR ($CDCl_3$) δ: 3.08 (s, 6H), 3.69–3.81 (m, 6H), 3.91 (t, J = 4.8 Hz, 2H), 4.24 (t, J = 4.8 Hz, 2H), 4.49 (t, J = 4.5 Hz, 1H), 4.65 (t, J = 4.5 Hz, 1H), 6.69 (s, 1H), 6.76 (d, J = 9.0 Hz, 2H), 7.27–7.33 (m, 1H), 7.48 (d, J = 9.0 Hz, 1H), 7.59 (d, J = 2.2, 1H), 7.81 (d, J = 9.0 Hz, 2H). EI-MS m/z 415 (M^+).

2.1.13. 6-Hydroxy-4^{I}-nitroflavone (9)

The same reaction as described above to prepare 6 was used, and 560 mg of 9 was obtained from 3 and BBr_3. EI-MS m/z 283 (M^+).

2.1.14. 6-(2-Hydroxy-ethoxy)-4^{I}-nitroflavone (10a)

The same reaction as described above to prepare 7a was used, and 40 mg of 10a was obtained from 9 in a yield of 9.9%. ^{1}H NMR (300 MHz, $CDCl_3$) δ: 3.88–4.02 (m, 2H), 4.13–4.20 (m, 2H), 6.89 (s, 1H), 7.38–7.41 (m, 1H), 7.59 (d, J = 9.3 Hz, 1H), 7.67 (d, J = 3.3 Hz, 1H), 8.12 (d, J = 9.0 Hz, 2H), 8.46 (d, J = 9.0 Hz, 2H).

2.1.15. 6-(2-(2-Hydroxy-ethoxy)-ethoxy)-4^{I}-nitroflavone (10b)

The same reaction as described above to prepare 7b was used, and 830 mg of 10b was obtained from 9. ^{1}H NMR (300 MHz, $CDCl_3$) δ: 3.70 (t, J = 5.1 Hz, 2H), 3.79 (s, 2H), 3.93 (t, J = 5.0 Hz, 2H), 4.28 (t, J = 4.8 Hz, 2H), 6.90 (s, 1H), 7.37–7.41 (m, 1H), 7.56 (d, J = 9.3 Hz, 1H), 7.66 (d, J = 3.3 Hz, 1H), 8.10 (d, J = 9.0 Hz, 2H), 8.40 (d, J = 9.0 Hz, 2H).

2.1.16. 6-(2-(2-(2-Hydroxy-ethoxy)-ethoxy)ethoxy)-4^{I}-nitroflavone (10c)

The same reaction as described above to prepare 7c was used, and 10c was obtained from 9 in a yield of 83.1%. ^{1}H NMR (300 MHz, $CDCl_3$) δ: 3.64 (t, J = 4.5 Hz, 2H), 3.71–3.78 (m, 6H), 3.93 (t, J = 4.8 Hz, 2H), 4.27 (t, J = 4.5 Hz, 2H), 6.90 (s, 1H), 7.38–7.42 (m, 1H), 7.55 (d, J = 9.0 Hz, 1H), 7.61 (d, J = 3.1 Hz, 1H), 8.10 (d, J = 8.7 Hz, 2H), 8.39 (d, J = 8.7 Hz, 2H). EI-MS m/z 415 (M^+).

2.1.17. 6-(2-Fluoro-ethoxy)-4^{I}-nitroflavone (11)

The same reaction as described above to prepare 8a was used, and 24 mg of 11 was obtained from 10a in a yield of 41.6%. ^{1}H NMR (300 MHz, $CDCl_3$) 4.26–4.41 (m, 2H), 4.71–4.92 (m, 2H), 6.91 (s, 1H), 7.42–7.44 (m, 1H), 7.56–7.61 (m, 2H), 8.11 (d, J = 9.0 Hz, 2H), 8.39 (d, J = 9.3 Hz, 2H).

2.1.18. 6-(2-Fluoro-ethoxy)-4^{I}-aminoflavone (12)

The same reaction as described above to prepare 4 was used, and 22 mg of 12 was obtained from 11 in a yield of 41.6%. ^{1}H NMR (300 MHz, $CDCl_3$) 4.10 (s, 2H), 4.27–4.39 (m, 2H), 4.71–4.88 (m, 2H), 6.70 (s, 1H), 6.76 (d, J = 9.0 Hz, 2H), 7.29–7.35 (m, 1H), 7.49 (d, J = 9.3 Hz, 1H), 7.58 (s, 1H), 7.75 (d, J = 9.0 Hz, 2H). EI-MS m/z 299 (M^+).

2.1.19. 6-(2-Fluoro-ethoxy)-4^{I}-methylaminoflavone (13)

To a solution of 12 (22 mg, 0.07 mmol) in DMSO (2 mL) were added methyl iodide (0.14 mL) and K_2CO_3 (50.8 mg, 0.37 mmol). The reaction mixture was stirred at room temperature for 5 h, and poured into water (30 mL). After extraction with ethyl acetate (2 30 mL), the organic layers were combined and dried over Na_2SO_4. Evaporation of the solvent afforded a residue, which was purified by reversed phase HPLC (acetonitrile/H_2O = 3:2) to give 10 mg of 13 (43.4% yield). ^{1}H NMR (300 MHz, $CDCl_3$) 2.93 (s, 3H), 4.22 (s, 1H), 4.26–4.40 (m, 2H), 4.70–4.91 (m, 2H), 6.71 (s, 1H), 6.76 (d, J = 9.0 Hz, 2H), 7.29–7.35 (m, 1H), 7.50 (d, J = 9.3 Hz, 1H), 7.58 (s, 1H), 7.78 (d, J = 8.7 Hz, 2H). EI-MS m/z 313 (M^+).

2.1.20. 6-(2-(2-Hydroxy-ethoxy)-ethoxy)-4^{I}-aminoflavone (14b)

The same reaction as described above to prepare 4 was used, and 251 mg of 14b was obtained from 10b in a yield of 37.9%. ^{1}H NMR ($CDCl_3$) δ: 3.69 (t, J = 5.1 Hz, 2H), 3.79 (s, 2H), 3.91 (t, J = 4.5 Hz, 2H), 4.09 (s, 2H), 4.27 (t, J = 4.2 Hz, 2H), 6.69 (s, 1H), 6.76 (d, J = 8.7 Hz, 2H), 7.27–7.32 (m, 1H), 7.48 (d, J = 9.3 Hz, 1H), 7.65 (d, J = 3.0 Hz, 1H), 7.75 (d, J = 8.4 Hz, 2H). EI-MS m/z 387 (M^+).

2.1.21. 6-(2-(2-(2-Hydroxy-ethoxy)-ethoxy)ethoxy)-4^{I}-aminoflavone (14c)

The same reaction as described above to prepare 4 was used, and 553 mg of 14c was obtained from 10c in a yield of 58.8%. ^{1}H NMR (300 MHz, $CDCl_3$) δ: 3.62–3.65 (m, 2H), 3.71–3.78 (m, 6H), 3.91 (t, J = 4.8 Hz, 2H), 4.11 (s, 2H), 4.25 (t, J = 4.5 Hz, 2H), 6.68 (s, 1H), 6.75 (d, J = 8.7 Hz, 2H), 7.27–7.32 (m, 1H), 7.50 (d, J = 9.0 Hz, 1H), 7.59 (d, J = 2.2 Hz, 1H), 7.74 (d, J = 8.7 Hz, 2H). EI-MS m/z 387 (M^+).

2.1.22. 6-(2-(2-Fluoro-ethoxy)-ethoxy)-4′-aminoflavone (15b)

The same reaction as described above to prepare 8b was used, and 10 mg of 15b was obtained from 14b in a yield of 9.1%. ^{1}H NMR ($CDCl_3$) δ: 3.79 (t, J = 4.2 Hz, 1H), 3.86–3.95 (m, 3H), 4.11 (s, 2H), 4.25 (t, J = 4.5 Hz, 2H), 4.53 (t, J = 4.2 Hz, 1H), 4.70 (t, J = 4.2 Hz, 1H), 6.68 (s, 1H), 6.75 (d, J = 9.0 Hz, 2H), 7.28–7.33 (m, 1H), 7.47 (d, J = 9.0 Hz, 1H), 7.58 (d, J = 3.0 Hz, 1H), 7.74 (d, J = 8.4 Hz, 2H). EI-MS m/z 343 (M^+).

2.1.23. 6-(2-(2-(2-Fluoro-ethoxy)-ethoxy)ethoxy)-4′-aminoflavone (15c)

The same reaction as described above to prepare 8 was used, and 85 mg of 15c was obtained from 14 in a yield of 81.3%. ^{1}H NMR ($CDCl_3$) δ: 3.62–3.65 (m, 2H), 3.70–3.78 (m, 7H), 3.82 (t, J = 3.9 Hz, 1H), 3.90 (t, J = 4.5 Hz, 2H), 4.22 (t, J = 4.5 Hz, 2H), 4.49 (t, J = 4.2 Hz, 1H), 4.66 (t, J = 4.2 Hz, 1H), 6.68 (s, 1H), 6.75 (d, J = 8.7 Hz, 2H), 7.27–7.32 (m, 1H), 7.46 (d, J = 9.3 Hz, 1H), 7.57 (d, J = 2.2 Hz, 1H), 7.73 (d, J = 8.7 Hz, 2H).

2.1.24. 6-(2-(2-Hydroxy-ethoxy)-ethoxy)-4′-methylaminoflavone (16b)

The same reaction as described above to prepare 13 was used, and 41 mg of 16b was obtained from 14b in a yield of 37.9%. ^{1}H NMR ($CDCl_3$) δ: 3.49 (s, 3H), 3.69 (t, J = 3.6 Hz, 2H), 3.77–3.79 (m, 2H), 3.91 (t, J = 4.8 Hz, 2H), 4.27 (t, J = 4.0 Hz, 2H), 6.65 (s, 1H), 6.68–6.69 (m, 2H), 7.29–7.32 (m, 1H), 7.47 (d, J = 9.0 Hz, 1H), 7.65 (d, J = 3.0 Hz, 1H), 7.78 (d, J = 9.0 Hz, 2H). EI-MS m/z 355 (M^+).

2.1.25. 6-(2-(2-(2-Hydroxy-ethoxy)-ethoxy)ethoxy)-4′-methylaminoflavone (16c)

The same reaction as described above to prepare 13 was used, and 145 mg of 16c was obtained from 14c in a yield of 64.8%. ^{1}H NMR ($CDCl_3$) δ: 2.92 (d, J = 3.0 Hz, 3H), 3.63 (t, J = 5.4 Hz, 2H) 3.72–3.76 (m, 6H), 3.91 (t, J = 5.1 Hz, 2H), 4.25 (t, J = 4.8 Hz, 3H), 6.65 (s, 1H), 6.68 (s, 2H), 7.28–7.32 (m, 1H), 7.46 (d, J = 9.3 Hz, 1H), 7.59 (d, J = 2.2 Hz, 1H), 7.77 (d, J = 8.7 Hz, 2H).

2.1.26. 6-(2-(2-Fluoro-ethoxy)-ethoxy)-4′-methylaminoflavone (17b)

The same reaction as described above to prepare 8 was used, and 9 mg of 17b was obtained from 16b in a yield of 21.9%. ^{1}H NMR ($CDCl_3$) δ: 2.93 (d, J = 5.1 Hz, 3H), 3.79 (t, J = 4.2 Hz, 1H), 3.85–3.95 (m, 3H), 4.26 (t, J = 4.8 Hz, 3H), 4.53 (t, J = 4.2 Hz, 1H), 4.70 (t, J = 4.5 Hz, 1H), 6.65 (s, 1H), 6.68 (s, 2H), 7.28–7.32 (m, 1H), 7.47 (d, J = 9.0 Hz, 1H), 7.59 (d, J = 3.0 Hz, 1H), 7.78 (d, J = 9.0 Hz, 2H). EI-MS m/z 357 (M^+).

2.1.27. 6-(2-(2-(2-Fluoro-ethoxy)-ethoxy)ethoxy)-4′-methylaminoflavone (17c)

The same reaction as described above to prepare 8 was used, and 20 mg of 17c was obtained from 16c in a yield of 13.8%. ^{1}H NMR ($CDCl_3$) δ: 2.92 (d, J = 4.8 Hz, 3H), 3.69–3.76 (m, 5H), 3.82 (t, J = 4.5 Hz, 1H), 3.91 (t, J = 4.8 Hz, 2H), 4.25 (t, J = 4.2 Hz, 3H), 4.50 (t, J = 4.2 Hz, 1H), 4.66 (t, J = 4.5 Hz, 1H), 6.65 (s, 1H), 6.68 (s, 2H), 7.28–7.31 (m, 1H), 7.46 (d, J = 9.3 Hz, 1H), 7.59 (d, J = 3.0 Hz, 1H), 7.77 (d, J = 8.7 Hz, 2H). EI-MS m/z 401 (M^+).

2.1.28. 4-Nitrobenzoic acid 2-acetyl-4-fluorophenyl ester (18)

The same reaction as described above to prepare 1 was used, and 2.5 g of 18 was obtained from 2-hydroxy-5-fluoroacetophenone and 4-nitrobenzoyl chloride in a yield of 85.6%. ^{1}H NMR (300 MHz, $CDCl_3$) δ: 2.56 (s, 3H), 7.23–7.34 (m, 2H), 7.56–7.60 (m, 1H), 8.37 (s, 4H).

2.1.29. 1-(5-Fluoro-2-hydroxyphenyl)-3-(4-nitrophenyl)propane-1,3-dione (19)

The same reaction as described above to prepare 2 was used, and 2.5 g of 19 was obtained from 18 in a yield of 96.3%. ^{1}H NMR (300 MHz, $CDCl_3$) δ: 6.81 (s, 2H), 7.02 (d, J = 9.0 Hz, 1H), 7.45 (d, J = 9.0 Hz, 1H), 7.68 (s, 1H), 8.11 (d, J = 8.7 Hz, 2H), 8.36 (d, J = 8.7 Hz, 2H), 11.7 (s, 1H).

2.1.30. 6-Fluoro-4′-nitroflavone (20)

The same reaction as described above to prepare 3 was used, and 2.0 g of 20 was obtained from 19 in a yield of 85.3%. EI-MS m/z 285 (M^+).

2.1.31. 6-Fluoro-4′-aminoflavone (21)

The same reaction as described above to prepare 4 was used, and 944 mg of 21 was obtained from 20 in a yield of 67.4%. ^{1}H NMR (300 MHz, $CDCl_3$) δ: 4.13 (s, broad, 2H), 6.74 (s, 1H), 6.76 (d, J = 9.0 Hz, 2H), 7.35–7.42 (m, 1H), 7.51–7.56 (m, 1H), 7.75 (d, J = 8.7 Hz, 2H), 7.82–7.85 (m, 1H).

2.1.32. 6-Fluoro-4′-methylaminoflavone (22)

To a mixture of 21 (300 mg, 1.2 mmol) and paraformaldehyde (179 mg, 5.9 mmol) in MeOH (15 mL) was added a solution of NaOMe (0.34 mL, 28 wt % in MeOH) dropwise at 0 C. The mixture was stirred under reflux for 1 h. After addition of $NaBH_4$ (246 mg, 6.5 mmol), the solution was heated under reflux for 45 min. To the cold mixture, 1 M NaOH was added followed by extraction with $CHCl_3$. The organic phase was dried over Na_2SO_4 and filtered. The solvent was removed, and the residue was purified by silica gel chromatography (hexane/ethyl acetate = 5:3) to give 314 mg of 22 (99.2%). ^{1}H NMR (300 MHz, $CDCl_3$) δ: 2.91 (s, 3H), 4.37 (s, broad, 1H), 6.63 (s, 1H), 6.66 (s, 2H), 7.32–7.39 (m, 1H), 7.49–7.53 (m, 1H), 7.74 (d, J = 8.7 Hz, 2H), 7.82–7.85 (m, 1H).

2.1.33. 6-Fluoro-4′-dimethylaminoflavone (23)

The same reaction as described above to prepare 5 was used, and 203 mg of 23 was obtained from 21 in a yield of 61.0%. ^{1}H NMR (300 MHz, $CDCl_3$) δ: 3.08 (s, 6H), 6.69 (s, 1H), 6.76 (d, J = 9.3 Hz, 2H), 7.35–7.41 (m, 1H), 7.51–7.56 (m, 1H), 7.81 (d, J = 9.0 Hz, 2H), 7.83–7.86 (m, 1H).

2.1.34. 6-(2-Tosyloxyethoxy)-4′-dimethylaminoflavone (24a)

To a solution of 8a (136 mg, 0.28 mmol) in pyridine (4 mL) was added tosyl chloride (122 mg, 0.65 mmol) in an ice bath. The reaction mixture was stirred for 32 h at room temperature following the reaction in an ice bath for 1 h. The organic phase was dried over Na_2SO_4 and filtered. The solvent was removed, and the residue was purified by silica gel chromatography (chloroform/MeOH = 20:1) to give 50 mg of 24a (36.8%). ^{1}H NMR (300 MHz, $CDCl_3$) δ: 2.45 (s, 3H), 3.07 (s, 6H), 4.23 (t, 2H, J = 4.5 Hz), 4.41 (t, J = 5.1 Hz, 2H), 6.68 (s, 1H), 6.75 (d, J = 9.0 Hz, 2H), 7.12–7.18 (m, 1H), 7.35 (d, J = 8.1 Hz, 2H), 7.43–7.56 (m, 2H), 7.82 (t, J = 9.0 Hz, 4H). EI-MS: m/z 479 [M^+].

2.1.35. 6-(2-(2-Tosyloxyethoxy)ethoxy)-4′-dimethylaminoflavone (24b)

The same reaction as described above to prepare 24a was used, and 111 mg of 24b was obtained from 8b in a yield of 34.1%. ^{1}H NMR (300 MHz, $CDCl_3$) δ: 2.41 (s, 3H), 3.08 (s, 6H), 3.76–3.85 (m, 4H), 4.12 (t, J = 5.1 Hz, 2H), 4.22 (t, J = 5.1 Hz, 2H), 6.70 (s, 1H), 6.76 (d, J = 9.0 Hz, 2H), 7.25–7.33 (m, 3H), 7.47 (d, J = 9.0 Hz, 1H), 7.55 (d, J = 3.0 Hz, 1H), 7.79–7.83 (m, 4H). EI-MS m/z 523 (M^+).

2.1.36. 6-(2-(2-(2-Tosyloxyethoxy)ethoxy)ethoxy)-4′-dimethylaminoflavone (24c)

The same reaction as described above to prepare 24a was used, and 35 mg of 24c was obtained from 8c in a yield of 39.9%. ^{1}H NMR (300 MHz, $CDCl_3$) δ: 2.43 (s, 3H), 3.08 (s, 6H), 3.62–3.73 (m, 6H), 3.87 (t, J = 4.8 Hz, 2H), 4.16–4.21 (m, 4H), 6.70 (s, 1H), 6.76 (d, J = 9.0 Hz, 2H), 7.28–7.33 (m, 3H), 7.47 (d, J = 9.0 Hz, 1H), 7.60 (d, J = 2.2 Hz, 1H), 7.79–7.83 (m, 4H). EI-MS m/z 567 (M^+).

2.2. Radiolabeling

[^{18}F]Fluoride produced by an ultracompact cyclotron (CYPRIS model 325R; Sumitomo Heavy Industry Ltd) via an $^{18}O(p,n)^{18}F$ reaction was adsorbed to a strong-base anion exchange resin (Bio-Rad), and was eluted with 500 μL of K_2CO_3 solution (33 mM) into 1 mL of acetonitrile containing Kryptofix 222 (K222) (20 mg). The solvent was removed azeotropically with anhydrous acetonitrile at 120 C under a nitrogen stream. A solution of tosylate precursor 24(a–c) (0.2 mg) in 400 μL of DMSO was added to the reaction vessel containing [^{18}F]Fluoride. The mixture was heated at 160 C for 5 min. The reaction mixture was purified by the reversed phase HPLC system (a Shimadzu LC-6A isocratic pump, a Shimadzu SPD-6A UV detector and an Aloka NDW-351D scitillation detector) on a YMC Hydrosphere C18 column (20 150 mm) with acetonitrile/water (70:30) at a flow rate of 9.0 mL/min to obtain [^{18}F]8(a–c). The radiochemical purity and specific activity were determined by analytical HPLC on a YMC Pack Pro C18 column (4.6 150 mm, acetonitrile/water (60:40), 1.0 mL/min).

2.3. Binding assays using the aggregated Ab peptide in solution

A solid form of Aβ(1-42) was purchased from Peptide Institute (Osaka, Japan). Aggregation of peptides was carried out by gently dissolving the peptide (0.25 mg/mL) in a buffer solution (pH 7.4) containing 10 mM sodium phosphate and 1 mM EDTA. The solutions were incubated at 37 C for 42 h with gentle and constant

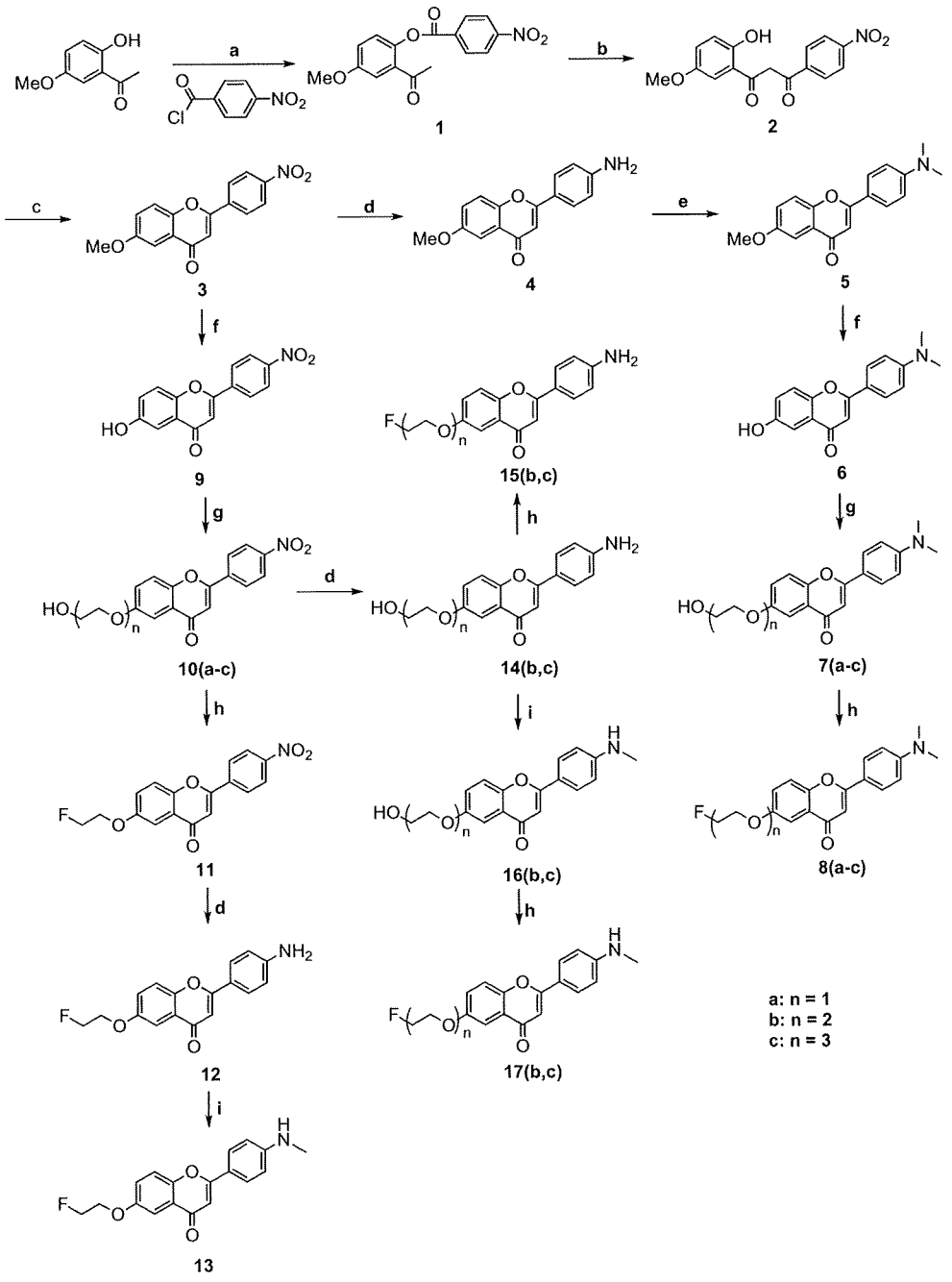

Scheme 1. Reagents: (a) pyridine; (b) KOH, pyridine; (c) H_2SO_4, AcOH; (d) EtOH, $SnCl_2$; (e) $(CH_2O)_n$, $NaCNBH_3$, AcOH; (f) CH_2Cl_2, BBr_3; (g) $Cl(CH_2CH_2O)_nH$ (n = 1–3) K_2CO_3, DMF; (h) DAST, DME; (i) DMSO, CH_3I, K_2CO_3.

shaking. Binding experiments were carried out as described previously.[14] [^{125}I]DMFV ([^{125}I]6-iodo-4′-dimethylaminoflavone) with 81.4 TBq/mmol specific activity and greater than 95% radiochemical purity was prepared using the standard iododestannylation reaction.[14] A mixture containing 50 μL of test compounds (0.2 pM-400 μM in 10% EtOH), 50 μL of 0.02 nM [^{125}I]DMFV, 50 μL of Aβ(1-42) aggregates and 850 μL of 10% EtOH was incubated at room temperature for 3 h. The mixture was then filtered through Whatman GF/B filters using a Brandel M-24 cell harvester, and the radioactivity on the filters containing the bound ^{125}I ligand was measured in a gamma counter (Aloka, ARC-380). Values for the half-maximal inhibitory concentration (IC_{50}) were determined from displacement curves of three independent experiments using GraphPad Prism 4.0, and those for the inhibition constant (K_i) were calculated using the Cheng-Prusoff equation:[18] $K_i = IC_{50}/(1 + [L]/K_d)$, where [L] is the concentration of [^{125}I]DMFV used in the assay, and K_d is the dissociation constant of DMFV (12.3 nM).[14]

2.4. Staining of amyloid plaques in transgenic mouse brain sections

Animal studies were conducted in accordance with institutional guidelines and approved by the Kyoto University Animal Care Committee. Tg2576 transgenic mice (female, 20-month-old) were used as an Alzheimer's model. While under isoflurane anesthesia, the mice were sacrificed by decapitation, and the brains were immediately removed and frozen in powdered dry ice. The frozen blocks were sliced into serial sections 10 μm thick using a cryostat (Leica Instruments, CM1900). Each slide was incubated with a 50% ethanol solution (100 μM) of compound 8a, 8b, or 8c, which have the characteristics to emit fluorescence. The sections were washed in 50% ethanol for 3 min two times, and examined using a microscope (Nikon, Eclipse 80i) equipped with a B-2A filter set (excitation, 450–490 nm; dichronic mirror, 505 nm; longpass filter, 520 nm). Thereafter, the serial sections were also immunostained with DAB as a chromogen using monoclonal antibodies against β-amyloid (Amyloid β-Protein Immunohistostain kit, WAKO).

2.5. In vivo biodistribution in normal mice

A saline solution (100 μL) containing ethanol (5 μL) of radiolabeled agents (18.5 kBq) was injected directly into a tail vein of ddY mice (5-week-old, 22–25 g). While under isoflurane anesthesia, the mice were sacrificed at various time points postinjection. The organs of interest were removed and weighed, and radioactivity was measured with an automatic gamma counter (Packard Cobra Auto-Gamma Counter 5003).

3. Results and discussion

The target FPEG flavone derivatives were prepared as shown in Scheme 1. The most common method of synthesizing flavones is known as the Baker-Venkataraman transformation.[19] In this process, a hydroxyacetophenone is first converted into a benzoyl ester 1, and this species is then treated with a base, forming a 1,3-diketone 2. Treatment of this diketone with acid leads to generation of the desired flavone 3. In the route for the synthesis of dimethylamino derivatives, the free amino derivative 4 was readily prepared from 3 by reduction with $SnCl_2$. Compound 5 was converted to 6 by demethylation with BBr_3 in CH_2Cl_2. To prepare compounds with 1-3 ethoxy groups as the PEG linkage, commercially available chlorides were coupled with the OH group of 6 to obtain 7(a–c), respectively. The fluorinated flavones, 8(a–c), were successfully obtained by reacting 7(a–c) with DAST in DME or ethylene glycol dimethyl ether. In the route for the synthesis of monomethylated derivatives and the primary amino derivatives, the demethylation of 3 with BBr_3 and the introduction of 1-3 ethoxy groups into 9 gave 10(a–c). To prepare

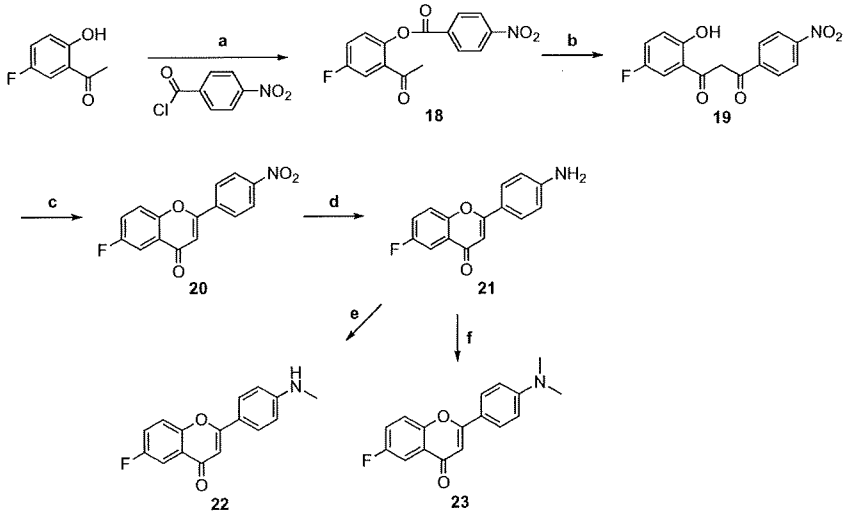

Scheme 2. Reagents: (a) pyridine; (b) KOH, pyridine; (c) H_2SO_4, AcOH; (d) EtOH, $SnCl_2$; (e) $(CH_2O)_n$, NaOMe, $NaBH_4$; (f) $(CH_2O)_n$, $NaCNBH_3$, AcOH.

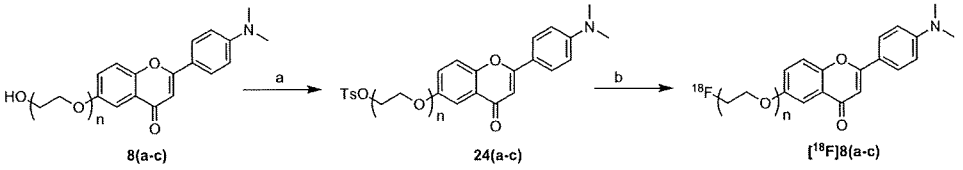

Scheme 3. Reagents: (a) tosyl chloride, pyridine; (b) K_2CO_3, [^{18}F]F , kryptofix[222], DMSO/acetonitrile.

the FPEG flavone with one ethoxy group (n = 1) (12 and 13), the fluorination of 10a with DAST, the reduction of 11 with $SnCl_2$ and the methylation of 12 were performed. The primary amino derivatives of FPEG flavones (n = 2 and 3) (15b and 15c) were synthesized by the fluorination of 14b and 14c with DAST following the reduction of the nitro group in 10b and 10c. The monomethylated FPEG flavones (n = 2 and 3) (17b and 17c) were synthesized by the methylation of 16b and 16c following the fluorination of 14b and 14c with DAST. We successfully synthesized the flavone derivatives (21, 22, and 23) with fluorine directly bound to the phenyl group according to a procedure reported previously (Scheme 2). To make the desired ^{18}F-labeled FPEG flavones, [^{18}F]8(a–c), the tosylates 24(a–c) were employed as the precursors. The free OH groups of 8(a–c) were converted into tosylates by reacting with TsCl in the presence of pyridine to give 24(a–c) (Scheme 3). Each of the tosylates, 24(a–c), was mixed with [^{18}F]fluoride/potassium carbonate and Kryptofix 222 in DMSO and heated at 160 C for 5 min. The crude product was purified by HPLC (radiochemical purity >99%, radiochemical yield 5–13%, decay corrected). The total synthesis time was 70 min, and the specific activity was estimated to be 33.3–55.5 GBq/mmol at the end of synthesis.

Table 1
Inhibition constants (K_i, nM) of compounds for the binding of [^{125}I]DMFV to Aβ(1-42) aggregates[a]

Compound	K_i (nM)	Compound	K_i (nM)
8a	5.3 ± 0.8	15c	234.0 ± 60.6
8b	14.4 ± 2.5	17b	54.5 ± 10.3
8c	19.3 ± 4.0	17c	45.1 ± 5.8
12	234.3 ± 63.5	21	260.5 ± 43.3
13	99.0 ± 11.8	22	110.0 ± 47.4
15b	321.1 ± 74.4	23	73.9 ± 5.3

[a] Values are the mean ± standard error of the mean for 4–9 experiments.

Table 2
Biodistribution of ^{18}F-labeled flavones in normal mice[a]

Organ	2 min	10 min	30 min	60 min
[^{18}F]8a				
Blood	2.80 ± 0.41	2.71 ± 0.13	2.53 ± 0.17	3.25 ± 0.31
Brain	4.17 ± 0.77	3.62 ± 0.21	1.89 ± 0.13	2.19 ± 0.18
Bone	2.02 ± 0.53	2.83 ± 0.23	4.51 ± 0.55	6.21 ± 0.84
[^{18}F]8b				
Blood	2.09 ± 0.35	2.30 ± 0.07	2.50 ± 0.21	2.94 ± 0.27
Brain	3.54 ± 0.54	2.75 ± 0.21	2.00 ± 0.20	2.13 ± 0.10
Bone	1.13 ± 0.22	1.65 ± 0.10	2.42 ± 0.38	3.74 ± 0.30
[^{18}F]8c				
Blood	2.35 ± 0.54	1.50 ± 0.26	1.40 ± 0.04	1.88 ± 0.08
Brain	2.89 ± 0.74	2.23 ± 0.36	1.31 ± 0.14	1.37 ± 0.11
Bone	1.53 ± 0.52	2.38 ± 0.39	4.06 ± 0.49	5.21 ± 0.98

[a] Expressed as % of injected dose per gram. Each value represents the mean ± SD for 4–5 mice at each interval.

In vitro binding experiments to evaluate the affinity of the FPEG flavones for Aβ aggregates were carried out in solutions with [^{125}I]DMFV as the ligand. The affinity of flavone derivatives for Aβ aggregates varied from 5 to 321 nM (Table 1). The flavone derivatives had affinity for Aβ(1-42) aggregates in the following order: the dimethyamino derivatives (8a, 8b, 8c, and 23) > the monomethylamino derivatives (13, 17b, 17c, and 22) > the primary amino derivatives (12, 15b, 15c, and 21). The results of the binding experiments are consistent with those of previous reports.[14,20,21] The K_i values indicated that the affinity for Aβ(1-42) aggregates was affected by the substituted group at position 4′ in the flavone structure, not by the length of the PEG introduced into the flavone backbone. We selected the dimethylamino derivatives (8a, 8b, and 8c), which showed greater binding affinity than the monomethylamino derivatives and the primary amino derivatives, for additional study.

Three ^{18}F FPEG flavones ([^{18}F]8a, [^{18}F]8b, and [^{18}F]8c) were examined for their biodistribution in normal mice (Table 2). All three ligands displayed high uptake from the brain 2.89–4.17%ID/g, at 2 min postinjection, indicating a level sufficient for imaging. In addition, they displayed good clearance from the normal brain with 1.89, 2.00, and 1.31%ID/g at 30 min postinjection for [^{18}F]8a, [^{18}F]8b, and [^{18}F]8c, respectively. These values were equal to 45.3%, 56.5%, and 45.3% of the initial uptake peak for [^{18}F]8a, [^{18}F]8b, and [^{18}F]8c, respectively. A rapid initial uptake in normal brain coupled with a fast washout are highly desirable properties for β-amyloid-imaging probes, as they lead to a high signal to background ratio. [^{18}F]8(a–c) showed the bone uptake (3.74–6.21%ID/g) at 60 min postinjection, suggesting there may be in vivo defluorination. However, the free fluorine was not taken up by brain tissue; therefore, the interference from this free fluoride is expected to be relatively low for brain imaging.[22]

To confirm the affinity of FPEG chalcone derivatives for β-amyloid plaques in the brain, neuropathological fluorescent staining

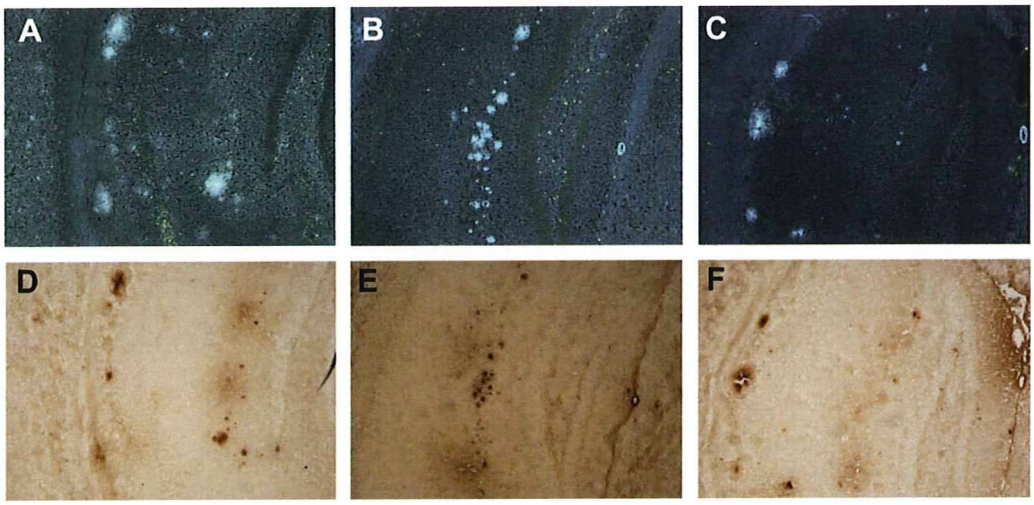

Figure 2. Neuropathological staining of flavone derivatives 8a (A), 8b (B), and 8c (C) in 10-μm brain sections of Tg2576 mice. Immunohistological staining with an antibody against β-amyloid (D, E, and F) in the adjacent sections of A, B, and C, respectively.

with 8a, 8b, and 8c was carried out using the Alzheimer's model (Fig. 2A–C). Many fluorescence spots were observed in the brain sections of Tg2576 transgenic (female, 20-month-old) mice, while no spots were observed in the brain sections of wild-type (female, 22-month-old) mice (data not shown). The fluorescent labeling pattern was consistent with that obtained by immunohistochemical labeling with an antibody specific for Aβ (Fig. 2D–F), indicating that FPEG flavones show specific binding to β-amyloid plaques in the mouse brain.

In conclusion, we successfully designed and synthesized novel ^{18}F labeled flavones with the FPEG strategy for PET imaging of β-amyloid in the brain. The affinity of the derivatives for Aβ aggregates varied from 5 to 321 nM. When in vitro plaque labeling was carried out using sections of brain from Tg2576 mice, FPEG flavones intensely stained β-amyloid plaques. In addition, they displayed good uptake into and a rapid washout from the brain after injection in normal mice. The combination of high binding affinity for β-amyloid plaques, high brain uptake, and good clearance in mice of the FPEG-flavone derivatives may provide a series of promising in vivo amyloid imaging agents for PET.

Acknowledgments

This study was supported by the Industrial Technology Research Grant Program from the New Energy and Industrial Technology Development Organization (NEDO) of Japan, and the Program for Promotion of Fundamental Studies in Health Sciences of the National Institute of Biomedical Innovation (NIBIO).

References and notes

1. Hardy, J. A.; Higgins, G. A. Science 1992, 256, 184.
2. Selkoe, D. J. Physiol. Rev. 2001, 81, 741.
3. Selkoe, D. J. Nat. Biotechnol. 2000, 18, 823.
4. Mathis, C. A.; Wang, Y.; Klunk, W. E. Curr. Pharm. Des. 2004, 10, 1469.
5. Nordberg, A. Lancet Neurol. 2004, 3, 519.
6. Ono, M.; Wilson, A.; Nobrega, J.; Westaway, D.; Verhoeff, P.; Zhuang, Z. P.; Kung, M. P.; Kung, H. F. Nucl. Med. Biol. 2003, 30, 565.
7. Verhoeff, N. P.; Wilson, A. A.; Takeshita, S.; Trop, L.; Hussey, D.; Singh, K.; Kung, H. F.; Kung, M. P.; Houle, S. Am. J. Geriatr. Psychiat. 2004, 12, 584.
8. Mathis, C. A.; Wang, Y.; Holt, D. P.; Huang, G. F.; Debnath, M. L.; Klunk, W. E. J. Med. Chem. 2003, 46, 2740.
9. Klunk, W. E.; Engler, H.; Nordberg, A.; Wang, Y.; Blomqvist, G.; Holt, D. P.; Bergstrom, M.; Savitcheva, I.; Huang, G. F.; Estrada, S.; Ausen, B.; Debnath, M. L.; Barletta, J.; Price, J. C.; Sandell, J.; Lopresti, B. J.; Wall, A.; Koivisto, P.; Antoni, G.; Mathis, C. A.; Langstrom, B. Ann. Neurol. 2004, 55, 306.
10. Kudo, Y.; Okamura, N.; Furumoto, S.; Tashiro, M.; Furukawa, K.; Maruyama, M.; Itoh, M.; Iwata, R.; Yanai, K.; Arai, H. J. Nucl. Med. 2007, 48, 553.
11. Agdeppa, E. D.; Kepe, V.; Liu, J.; Flores-Torres, S.; Satyamurthy, N.; Petric, A.; Cole, G. M.; Small, G. W.; Huang, S. C.; Barrio, J. R. J. Neurosci. 2001, 21, RC189.
12. Shoghi-Jadid, K.; Small, G. W.; Agdeppa, E. D.; Kepe, V.; Ercoli, L. M.; Siddarth, P.; Read, S.; Satyamurthy, N.; Petric, A.; Huang, S. C.; Barrio, J. R. Am. J. Geriatr. Psychiat. 2002, 10, 24.
13. Rowe, C. C.; Ackerman, U.; Browne, W.; Mulligan, R.; Pike, K. L.; O'Keefe, G.; Tochon-Danguy, H.; Chan, G.; Berlangieri, S. U.; Jones, G.; Dickinson-Rowe, K. L.; Kung, H. P.; Zhang, W.; Kung, M. P.; Skovronsky, D.; Dyrks, T.; Holl, G.; Krause, S.; Friebe, M.; Lehman, L.; Lindemann, S.; Dinkelborg, L. M.; Masters, C. L.; Villemagne, V. L. Lancet Neurol. 2008, 7, 129.
14. Ono, M.; Yoshida, N.; Ishibashi, K.; Haratake, M.; Arano, Y.; Mori, H.; Nakayama, M. J. Med. Chem. 2005, 48, 7253.
15. Stephenson, K. A.; Chandra, R.; Zhuang, Z. P.; Hou, C.; Oya, S.; Kung, M. P.; Kung, H. F. Bioconjugate Chem. 2007, 18, 238.
16. Ono, M.; Kung, M. P.; Hou, C.; Kung, H. F. Nucl. Med. Biol. 2002, 29, 633.
17. Zhuang, Z. P.; Kung, M. P.; Wilson, A.; Lee, C. W.; Plossl, K.; Hou, C.; Holtzman, D. M.; Kung, H. F. J. Med. Chem. 2003, 46, 237.
18. Cheng, Y.; Prusoff, W. Biochem. Pharmacol. 1973, 1973, 3099.
19. Ares, J. J.; Outt, P. E.; Randall, J. L.; Murray, P. D.; Weisshaar, P. S.; O'Brien, L. M.; Ems, B. L.; Kakodkar, S. V.; Kelm, G. R.; Kershaw, W. C., et al J. Med. Chem. 1995, 38, 4937.
20. Ono, M.; Haratake, M.; Mori, H.; Nakayama, M. Bioorg. Med. Chem. 2007, 15, 6802.
21. Ono, M.; Hori, M.; Haratake, M.; Tomiyama, T.; Mori, H.; Nakayama, M. Bioorg. Med. Chem. 2007, 15, 6388.
22. Zhang, W.; Oya, S.; Kung, M. P.; Hou, C.; Maier, D. L.; Kung, H. F. Nucl. Med. Biol. 2005, 32, 799.

Bioorganic & Medicinal Chemistry 17 (2009) 6402–6406

Contents lists available at ScienceDirect

Bioorganic & Medicinal Chemistry

journal homepage: www.elsevier.com/locate/bmc

Synthesis and biological evaluation of radioiodinated 2,5-diphenyl-1,3,4-oxadiazoles for detecting b-amyloid plaques in the brain

Hiroyuki Watanabe [a], Masahiro Ono [a,b,*], Ryoichi Ikeoka [a], Mamoru Haratake [a], Hideo Saji [b], Morio Nakayama [a,*]

[a] Graduate School of Biomedical Sciences, Nagasaki University, 1-14 Bunkyo-machi, Nagasaki 852-8521, Japan
[b] Graduate School of Pharmaceutical Sciences, Kyoto University, 46-29 Yoshida Shimoadachi-cho, Sakyo-ku, Kyoto 606-8501, Japan

article info

Article history:
Received 2 June 2009
Revised 10 July 2009
Accepted 11 July 2009
Available online 17 July 2009

Keywords:
Alzheimer's disease
β-Amyloid plaques
SPECT imaging

abstract

This paper describes the synthesis and biological evaluation of a new series of 2,5-diphenyl-1,3,4-oxadiazole (1,3,4-DPOD) derivatives for detecting β-amyloid plaques in Alzheimer's brains. The affinity for β-amyloid plaques was assessed by an in vitro binding assay using pre-formed synthetic Aβ42 aggregates. The new series of 1,3,4-DPOD derivatives showed affinity for Aβ42 aggregates with K_i values ranging from 20 to 349 nM. The 1,3,4-DPOD derivatives clearly stained β-amyloid plaques in an animal model of Alzheimer's disease, reflecting the affinity for Aβ42 aggregates in vitro. Compared to 3,5-diphenyl-1,2,4-oxadiazole (1,2,4-DPOD) derivatives, they displayed good penetration of and fast washout from the brain in biodistribution experiments using normal mice. The novel radioiodinated 1,3,4-DPOD derivatives may be useful probes for detecting β-amyloid plaques in the Alzheimer's brain.

1. Introduction

Alzheimer's disease (AD) is a progressive neurodegenerative disorder pathologically characterized by the deposition of β-amyloid (Aβ) peptides as senile plaques in the brain.[1,2] Since the deposition of Aβ plaques is an early event in the development of AD, a validated biomarker of Aβ deposition in the brain would likely prove useful for identifying and following individuals at risk for AD and assist in the evaluation of new anti-amyloid therapies currently under development. Therefore, the quantitative evaluation of Aβ plaques in the brain with non-invasive techniques such as positron emission tomography (PET) and single photon emission computed tomography (SPECT) could lead to the presymptomatic detection of AD and new anti-amyloid therapies.[3–5]

In the past few years, several groups have reported potential Aβ-imaging probes for the detection of Aβ plaques in vivo. Tracers such as [^{11}C]PIB,[6,7] [^{11}C]SB-13,[8,9] [^{18}F]BAY94-9172,[10] [^{11}C]BF-227,[11] [^{18}F]FDDNP,[12–14] and [^{123}I]IMPY[15–18] have been tested clinically and demonstrated utility. [^{123}I]IMPY is the only tracer for SPECT, the other five tracers are Aβ-imaging probes for PET. Since SPECT is more valuable than PET in terms of routine diagnostic use, the development of more useful Aβ-imaging agents for SPECT has been a critical issue.

Recently, we successfully designed and synthesized a new series of 3,5-diphenyl-1,2,4-oxadiazole (1,2,4-DPOD) derivatives as SPECT probes for the in vivo imaging of Aβ plaques in the brain.[19] The 1,2,4-DPOD derivatives are categorized into Aβ-imaging agents with the three-aromatic-ring linked system.[20–22] The derivatives displayed excellent affinity for Aβ aggregates in in vitro binding experiments. The degree to which the DPOD derivatives penetrated the brain was also very encouraging. However, nonspecific binding in vivo reflected by a slow washout from the normal mouse brain makes them unsuitable for the imaging of Aβ plaques. The less than ideal in vivo biodistribution results in normal mice indicate that there is a critical need to fine-tune the kinetics of brain uptake and washout. Additional structural changes, that is, reducing the lipophilicity, are necessary to improve the in vivo properties of the DPOD derivatives.

In an attempt to further develop novel ligands for the imaging of Aβ plaques in AD, we designed a series of 2,5-diphenyl-1,3,4-oxadiazole (1,3,4-DPOD) derivatives, which are structural isomers of 1,2,4-DPOD and less lipophilic than 1,2,4-DPOD (Fig. 1). To our

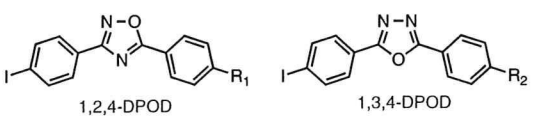

1,2,4-DPOD 1,3,4-DPOD

Figure 1. Chemical structure of 1,2,4-DPOD reported previously and 1,3,4-DPOD reported in this paper. R_1 = NH_2, $NHCH_3$, $N(CH_3)_2$, OCH_3, OH; R_2 = $N(CH_3)_2$, OCH_3, OH, OCH_2CH_2OH, $(OCH_2CH_2)_2OH$, $(OCH_2CH_2)_3OH$.

* Corresponding authors. Tel.: +81 75 753 4608; fax: +81 75 753 4568 (M.O.); tel./fax: +81 95 819 2441 (M.N.).
E-mail addresses: ono@pharm.kyoto-u.ac.jp (M. Ono), morio@nagasaki-u.ac.jp (M. Nakayama).

0968-0896/$ - see front matter
doi:10.1016/j.bmc.2009.07.020

knowledge, this is the first time the use of 1,3,4-DPOD derivatives in vivo as probes to image Aβ plaques in the AD brain has been proposed. Described herein is the synthesis of a novel series of 1,3,4-DPOD derivatives and the characterization as Aβ-imaging probes in comparison with 1,2,4-DPOD derivatives.

2. Results and discussion

The synthesis of 1,3,4-DPOD derivatives is outlined in Schemes 1 and 2. We used the one-pot synthesis method of producing 2,5-diphenyl-1,3,4-oxadiazoles.[23] The 2,5-diphenyl-1,3,4-oxadiazoles (3 and 4) were prepared by 4-iodobenzhydrazide with 4-dimethylaminobenzaldehyde and 4-methoxybenzaldehyde in the presence of ceric ammonium nitrate (CAN). Compound 4 was converted to 6 by demethylation with BBr_3 in CH_2Cl_2 (49% yield). Direct alkylation of 6 with ethylene chlorohydrin, ethylene glycol mono-2-chloroethyl ether, or 2-[2-(2-chloroethoxy)ethoxy]ethanol with potassium carbonate in DMF resulted in 7–9. The tributyltin derivatives (2 and 5) were prepared from corresponding compounds (1 and 4) using a halogen to tributyltin exchange reaction catalyzed by Pd(0) for yields of 8.2% and 6.5%, respectively. The tributyltin derivatives were used as the starting materials for radioiodination in the preparation of [^{125}I]3 and [^{125}I]4. Novel radioiodinated 1,3,4-DPOD derivatives were obtained by an iododestannylation reaction using hydrogen peroxide as the oxidant which produced the desired radioiodinated ligands (Scheme 3). It was anticipated that the no-carrier-added preparation would result in a final product bearing a theoretical specific activity similar to that of ^{125}I (2200 Ci/mmol). The radiochemical identity of the radioiodinated ligands was verified by co-injection with non-radioiodinated compounds from their HPLC profiles. [^{125}I]3 and [^{125}I]4 were each obtained in a radiochemical yield of >45% with a radiochemical purity of >95% after purification by HPLC.

The affinity of 1,3,4-DPOD derivatives (3, 4, 6–9) was evaluated based on inhibition of the binding of [^{125}I]IMPY to Aβ42 aggregates. As shown in Table 1, all 1,3,4-DPOD derivatives showed inhibitory activity toward Aβ aggregates. The affinity of 1,3,4-DPOD derivatives for Aβ aggregates varied from 20 to 349 nM. Compound 3 with the dimethylamino group and 4 with the methoxy group showed high binding affinity with a K_i of 20 and 46 nM, respectively, while no marked affinity was observed for 6–9. Compound 3 displayed almost equal affinity for Aβ aggregates as the 1,2,4-DPOD derivative with the dimethylamino group (4-(3-(4-iodophenyl)-1,2,4-oxadiazole-5-yl)-N,N-dimethylamine; 1,2,4-DPOD-DM, K_i = 15 nM).[19]

To confirm the affinity of 1,3,4-DPOD derivatives for Aβ plaques in the brain, fluorescent staining of sections of mouse brain from an animal model of AD was carried out with compound 3 (Fig. 2). Many fluorescence spots were observed in the brain sections of Tg2576 transgenic mice (female, 28-month-old) (Fig. 2A), while no spots were observed in the brain sections of wild-type mice (female, 28-month-old) (Fig. 2B). The fluorescent labeling pattern was consistent with that observed with thioflavin S (Fig. 2C). These results suggested that 3 shows specific binding to Aβ plaques in the mouse brain. In the fluorescent staining of Tg2576 mouse brain sections, 4 also showed specific binding to Aβ plaques in the brain (data not shown).

Next, [^{125}I]3 and [^{125}I]4 were evaluated for their in vivo biodistribution in normal mice. A biodistribution study provides critical information on brain penetration. Generally, a freely diffusible compound with an optimal log P value of 2 3 will have an initial brain uptake of 2 3% dose/whole brain at 2 min after iv injection. [^{125}I]3 and [^{125}I]4 examined in this study displayed optimal lipophilicity as reflected by log P values of 2.43 and 2.58, respectively (Table 2). As expected, these ligands displayed good brain uptake ranging from 3.8% to 5.9% ID/g brain at 2–10 min postinjection, indicating a level sufficient for brain imaging probes (Table 3). In addition, they displayed good clearance from the normal brain with 1.8% and 0.36% ID/g at 60 min postinjection for [^{125}I]3 and [^{125}I]4, respectively. These values were equal to a peak in brain uptake of 30% and 9.6%, respectively. Additionally, all of the other organs or tissues displayed a good initial uptake and a relatively fast washout with time. To directly compare the brain uptake and washout of [^{125}I]1,2,4-DPOD and [^{125}I]1,3,4-DPOD, a combined plot is presented in Figure 3. It is apparent that [^{125}I]1,2,4-DPOD showed a lower initial uptake with a longer retention, while [^{125}I]1,3,4-DPOD displayed a higher initial uptake but with a faster washout from the brain. At 2 or 10 min after iv injection, the uptake of [^{125}I]1,3,4-DPOD reached a maximum after which the activity in the normal brain was washed out. It is important to note that

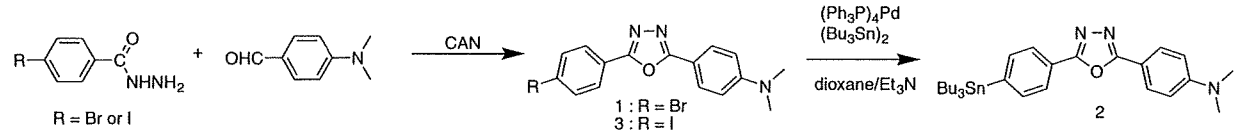

Scheme 1.

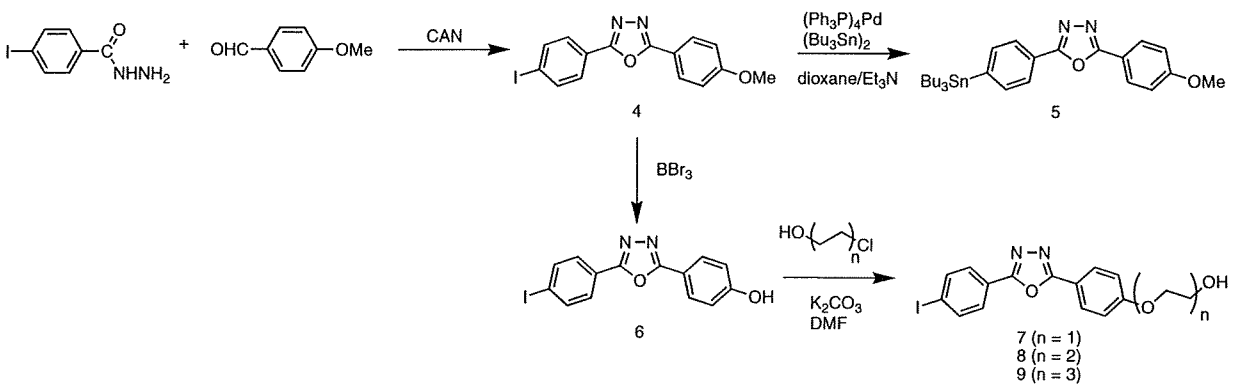

Scheme 2.

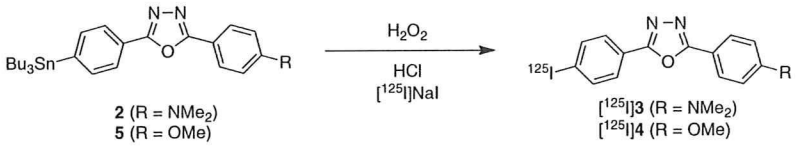

Scheme 3.

Table 1
Inhibition constants (K_i) for binding of 1,3,4-DPOD derivatives determined using [^{125}I]IMPY as the ligand in Aβ42 aggregates

Compound	K_i[a] (nM)
3	20.1 ± 2.5
4	46.1 ± 12.6
6	229.6 ± 47.3
7	282.2 ± 61.4
8	348.6 ± 51.7
9	257.7 ± 34.8

[a] Values are the mean ± standard error for the mean for 4–6 independent experiments.

Table 2
Partition coefficients for 1,2,4-DPOD and 1,3,4-DPOD derivatives

Compound	Log P[a]
3	2.43 ± 0.07
4	2.58 ± 0.06
1,2,4-DPOD-DM	3.22 ± 0.01
1,2,4-DPOD-OMe	3.37 ± 0.04

[a] Octanol/buffer (0.1 M phosphate-buffered saline, pH 7.4) partition coefficients. Each value represents the mean ± SD for 2–3 experiments.

Table 3
Biodistribution of radioactivity after injection of [^{125}I]1,3,4-DPOD derivatives in normal mice[a]

Tissue	Time after injection (min)			
	2	10	30	60
[^{125}I]3				
Blood	3.28 (0.46)	3.51 (0.29)	2.53 (0.28)	2.21 (0.41)
Liver	15.87 (3.49)	19.12 (2.43)	12.64 (2.44)	10.01 (1.64)
Kidney	9.14 (1.60)	7.80 (0.64)	5.71 (1.35)	3.81 (0.64)
Intestine	2.28 (0.55)	11.34 (1.61)	12.58 (2.35)	16.22 (2.51)
Spleen	3.56 (0.96)	4.10 (0.40)	2.63 (0.54)	2.05 (0.41)
Pancreas	5.32 (0.98)	4.39 (2.17)	2.50 (0.56)	2.14 (0.90)
Heart	3.99 (3.10)	3.55 (1.86)	2.03 (0.30)	1.54 (0.31)
Stomach[b]	1.40 (0.10)	4.73 (1.86)	4.79 (1.12)	5.50 (0.51)
Brain	2.98 (0.53)	5.93 (0.76)	3.16 (0.69)	1.78 (0.41)
[^{125}I]4				
Blood	1.84 (0.30)	1.60 (0.30)	1.26 (0.26)	0.80 (0.20)
Liver	9.60 (1.73)	12.60 (1.14)	8.07 (1.66)	4.65 (1.34)
Kidney	7.14 (1.46)	4.85 (0.48)	4.36 (1.12)	2.48 (0.37)
Intestine	2.07 (0.36)	4.49 (0.60)	10.06 (1.81)	19.85 (4.71)
Spleen	2.44 (0.28)	1.51 (0.26)	0.80 (0.10)	0.60 (0.26)
Pancreas	4.74 (0.63)	1.98 (0.37)	0.96 (0.03)	0.57 (0.14)
Heart	4.80 (1.33)	1.73 (0.27)	0.92 (0.25)	0.43 (0.11)
Stomach[b]	0.71 (0.13)	1.41 (0.91)	3.12 (0.90)	2.90 (1.57)
Brain	3.75 (0.78)	2.74 (0.37)	1.04 (0.14)	0.36 (0.13)

[a] Expressed as % injection dose per gram. Each value represents the mean (SD) for 4–6 animals.
[b] Expressed as % injected dose per organ.

the ideal Aβ-imaging agent should have good brain penetration to deliver the intended dose into the brain, while maintaining a fast washout from normal tissues. Because the normal brain has no Aβ plaques to trap the agent, the washout from the brain should also be fast. Once the high affinity ligand is delivered into the regions containing the Aβ plaques, imaging agents such as [^{125}I]3 and [^{125}I]4 are expected to be trapped in this region longer due to its high binding affinity. The differences between the kinetics in normal and Aβ plaque-containing regions will result in a higher signal to noise ratio (target to non-target ratio) in the AD brain. Based on the data presented for [^{125}I]1,3,4-DPOD, it is predicted that the brain trapping of [^{125}I]1,3,4-DPOD in Aβ-containing regions will be much better than that of [^{125}I]1,2,4-DPOD. The log P values of 1,3,4-DPOD derivatives (log P = 2.43 and 2.58 for 3 and 4, respectively) were lower than those of 1,2,4-DPOD derivatives (log P = 3.22 and 3.37 for 1,2,4-DPOD-DM and 1,2,4-DPOD-OMe, respectively). Although many factors such as molecular size, ionic charge, and lipophilicity affect the uptake of a compound into the brain, the difference in lipophilicity may be one reason for the difference in brain uptake and washout between 1,3,4-DPOD and 1,2,4-DPOD. Further structural modifications, that is, decreasing the lipophilicity by introducing the hydrophilic group, should improve the in vivo properties of 1,3,4-DPOD derivatives.

3. Conclusion

In conclusion, we successfully designed and synthesized a new series of 1,3,4-DPOD derivatives as probes for the in vivo imaging of Aβ plaques in the brain. In in vitro binding experiments, these 1,3,4-DPOD derivatives showed affinity for Aβ42 aggregates. The 1,3,4-DPOD derivatives clearly stained Aβ plaques in an animal model of AD, reflecting their affinity for Aβ aggregates in vitro. Compared to 1,2,4-DPOD, they displayed good penetration of and a fast washout from the brain in biodistribution experiments using

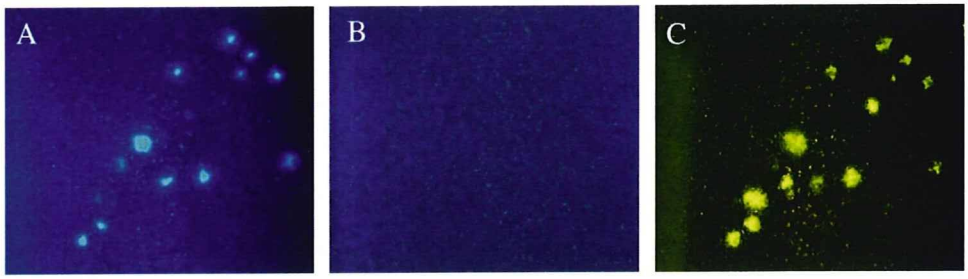

Figure 2. Neuropathological staining of compound 3 on 10-μm AD model mouse sections (A) and wild-type mouse sections (B). Labeled plaques were confirmed by staining of the adjacent sections with thioflavin S (C).

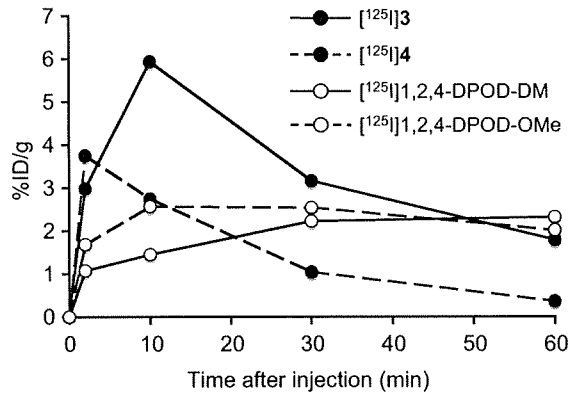

Figure 3. Comparison of brain uptake of [^{125}I]3, [^{125}I]4, [^{125}I]1,2,4-DPOD-DM and [^{125}I]1,2,4-DPOD-OMe in normal mice. The kinetics of the uptake of [^{125}I]3 and [^{125}I]4 may provide a better pattern for the localization of Aβ plaques in the brain.

normal mice. Taken together, the present results suggested that the novel radioiodinated 1,3,4-DPOD derivatives may be useful probes for detecting Aβ plaques in the AD brain.

4. Experimental

4.1. General

All reagents were commercial products and used without further purification unless otherwise indicated. ^{1}H NMR spectra were obtained on a Varian Gemini 300 spectrometer with TMS as an internal standard. Coupling constants are reported in hertz. Multiplicity is defined by s (singlet), d (doublet), t (triplet), and m (multiplet). ^{13}C NMR spectra were obtained on an AL400 JEOL spectrometer with TMS as an internal standard. Mass spectra were obtained on a JEOL IMS-DX.

4.1.1. 4-(5-(4-Bromophenyl)-1,3,4-oxadiazol-2-yl)-N,N-dimethylbenzenamine (1)

To a solution of 4-bromobenzhydrazide (215 mg, 1 mmol) and 4-dimethylaminobenzaldehyde (149 mg, 1 mmol) in dry CH_2Cl_2 (10 mL) was added CAN (548 mg, 1 mmol). The reaction mixture was stirred under reflux for 24 h. Water was added and following extraction with $CHCl_3$, the organic phase was dried over Na_2SO_4. The solvent was removed and the residue was purified by silica gel chromatography (hexane/ethyl acetate = 4:1) to give 12 mg of 1 (3.5%). ^{1}H NMR (300 MHz, $CDCl_3$) δ 3.08 (s, 6H), 6.76 (d, J = 9.0 Hz, 2H), 7.66 (d, J = 8.4 Hz, 2H), 7.98 (dd, J = 5.4, 4.5 Hz, 4H). MS m/z 362 (M^+).

4.1.2. 4-(5-(4-Tributylstannyl)phenyl)-1,3,4-oxadiazol-2-yl)-N,N-dimethylbenzenamine (2)

A mixture of 1 (19 mg, 0.06 mmol), bis(tributyltin) (0.04 mL) and $(Ph_3P)_4Pd$ (3 mg, 0.002 mmol) in a mixed solvent (6 mL, 1:1 dioxane/Et_3N) was stirred under reflux for 4.5 h. The solvent was removed, and the residue was purified by silica gel chromatography (hexane/ethyl acetate = 3:1) to give 2.5 mg of 2 (8.2%). ^{1}H NMR (300 MHz, $CDCl_3$) δ 0.87–1.6 (m, 27H), 3.07 (s, 6H), 6.77 (d, J = 9.0 Hz, 2H), 7.61 (d, J = 8.4 Hz, 2H), 8.01 (dd, J = 9.0, 8.1 Hz, 4H).

4.1.3. 4-(5-(Iodophenyl)-1,3,4-oxadiazol-2-yl)-N,N-dimethylbenzenamine (3)

The same reaction as described above to prepare 1 was used, and 14 mg of 3 was obtained in a 1.8% yield from 4-iodobenzohydrazide and 4-dimethylaminobenzaldehyde. ^{1}H NMR (300 MHz, $CDCl_3$) δ 3.07 (s, 6H), 6.76 (d, J = 3.0 Hz, 2H), 7.85 (d, J = 12.0 Hz, 4H), 7.97 (d, J = 3.0 Hz, 2H). ^{13}C NMR (400 MHz, $CDCl_3$) δ 40.1, 97.8, 110.7, 111.6, 123.9, 128.0, 128.4, 138.2, 152.5, 162.9, 165.5. HRMS m/z $C_{16}H_{14}N_3OI$ found 391.0191/ calcd 391.0182 (M^+).

4.1.4. 2-(4-Iodophenyl)-5-(4-methoxyphenyl)-1,3,4-oxadiazole (4)

The same reaction as described above to prepare 1 was used, and 40 mg of 4 was obtained in a 8.8% yield from 4-iodobenzohydrazide and 4-methoxybenzaldehyde. ^{1}H NMR (300 MHz, $CDCl_3$) δ 3.89 (s, 3H), 7.03 (d, J = 2.9 Hz, 2H), 7.86 (q, J = 7.8 Hz, 4H), 8.03 (d, J = 3.0 Hz, 2H). ^{13}C NMR (400 MHz, $CDCl_3$) δ 55.5, 98.2, 114.6, 116.2, 123.6, 128.1, 128.8, 138.3, 162.5, 163.6, 164.7. HRMS m/z $C_{15}H_{11}N_2O_2I$ found 377.9877, calcd 377.9865 (M^+).

4.1.5. 2-(4-(Tributylstannyl)phenyl)-5-(4-methoxyphenyl)-1,3,4-oxadiazole (5)

The same reaction as described above to prepare 2 was used, and 6 mg of 5 was obtained in a 6.5% yield from 4. ^{1}H NMR (300 MHz, $CDCl_3$) δ 0.87–1.58 (m, 27H), 3.91 (s, 3H), 7.04 (d, J = 3.1 Hz, 2H), 7.63 (d, J = 2.6 Hz, 2H), 8.06 (q, J = 6.6 Hz, 4H).

4.1.6. 4-(5-(4-Iodophenyl)-1,3,4-oxadiazol-2-yl)phenol (6)

BBr_3 (0.6 mL, 1 M solution in CH_2Cl_2) was added to a solution of 4 (36 mg, 0.1 mmol) in CH_2Cl_2 (16 mL) dropwise in an ice bath. The mixture was allowed to warm to room temperature and stirred for 5 days. Water (50 mL) was added while the reaction mixture was cooled in an ice bath. The mixture was extracted with $CHCl_3$ (30 mL) and the water layer was extracted with ethyl acetate. The organic phase was dried over Na_2SO_4 and filtered. The solvent was removed, and the residue was purified by silica gel chromatography (hexane/ethyl acetate = 2:1) to give 17 mg of 6 (49.0%). ^{1}H NMR (300 MHz, $CDCl_3$) δ 6.98–7.06 (m, 2H), 7.86–7.91 (m, 4H), 8.02–8.09 (m, 2H). HRMS m/z $C_{14}H_9N_2O_2I$ found 363.9712, calcd 363.9709 (M^+).

4.1.7. 2-(4-(5-(4-Iodophenyl)-1,3,4-oxadiazol-2-yl)phenoxy)ethanol (7)

A mixture of 6 (22 mg, 0.06 mmol), potassium carbonate (24.5 mg, 0.18 mmol) and ethylene chlorohydrin (4 μL, 0.06 mmol) in anhydrous DMF (3 mL) was stirred under reflux for 6.5 h. After cooling to room temperature, water was added, and the reaction mixture was extracted with $CHCl_3$. The organic layer was separated, dried over Na_2SO_4 and evaporated. The resulting residue was purified by silica gel chromatography (hexane/ethyl acetate = 2:3) to give 11 mg of 7 (44.6%). ^{1}H NMR (300 MHz, $CDCl_3$) δ 4.03 (q, J = 5.0 Hz, 2H), 4.18 (d, J = 3.0 Hz, 2H) 7.06 (d, J = 3.0 Hz, 2H), 7.87 (q, J = 8.0 Hz, 4H), 8.07 (d, J = 3.0 Hz, 2H). HRMS m/z $C_{16}H_{13}N_2O_3I$ found 407.9983, calcd 407.9971 (M^+).

4.1.8. 2-(2-(4-(5-(4-Iodophenyl)-1,3,4-oxadiazol-2-yl)phenoxy)ethoxy)ethanol (8)

The same reaction as described above to prepare 7 was used, and 9 mg of 8 was obtained in a 25.9% yield from 6 and ethylene glycol mono-2-chloroethyl ether. ^{1}H NMR (300 MHz, $CDCl_3$) δ 3.70 (t, J = 3.1 Hz, 2H), 3.79 (q, J = 4.8 Hz, 2H), 3.92 (t, J = 3.2 Hz, 2H), 4.23 (t, J = 3.1 Hz, 2H), 7.06 (d, J = 3.1 Hz, 2H), 7.87 (q, J = 7.6 Hz, 4H), 8.70 (d, J = 3.1 Hz, 2H). HRMS m/z $C_{18}H_{17}N_2O_4I$ found 452.0244, calcd 452.0233 (M^+).

4.1.9. 2-(2-(2-(4-(5-(4-Iodophenyl)-1,3,4-oxadiazol-2-yl)phenoxy)ethoxy)ethoxy)ethanol (9)

The same reaction as described above to prepare 7 was used, and 7.8 mg of 9 was obtained in a 44.7% yield from 6 and 2-[2-(chloroethoxy)ethoxy]ethanol. ^{1}H NMR (300 MHz, $CDCl_3$) δ 3.61–3.77 (m, 8H), 3.91 (t, J = 3.1 Hz), 4.23 (t, J = 3.2 Hz, 2H), 7.06 (d,

J = 3.0 Hz, 2H), 7.87 (q, J = 7.8 Hz, 4H), 8.06 (d, J = 2.3 Hz, 2H). HRMS m/z $C_{20}H_{21}N_2O_5I$ found 496.0525, calcd 496.0495 (M^+).

4.2. Iododestannylation reaction

The radioiodinated forms of compounds 3 and 4 were prepared from the corresponding tributyltin derivatives by iododestannylation. Briefly, to initiate the reaction, 50 μL of H_2O_2 (3%) was added to a mixture of a tributyltin derivative (50 μg/50 μL EtOH), [^{125}I]NaI (0.1–0.2 mCi, specific activity 2200 Ci/mmol), and 50 μL of 1 N HCl in a sealed vial. The reaction was allowed to proceed at room temperature for 3 min and terminated by addition of $NaHSO_3$. After neutralization with sodium biocarbonate and extraction with ethyl acetate, the extract was dried by passing through an anhydrous Na_2SO_4 column and then blown dry with a stream of nitrogen gas. The radioiodinated ligand was purified by HPLC on a Cosmosil C_{18} column with an isocratic solvent of H_2O/acetonitrile (4:6) at a flow rate of 1.0 mL/min.

4.3. Binding assays using the aggregated Ab peptide in solution

A solid form of Aβ42 was purchased from Peptide Institute (Osaka, Japan). Aggregation was carried out by gently dissolving the peptide (0.25 mg/mL) in a buffer solution (pH 7.4) containing 10 mM sodium phosphate and 1 mM EDTA. The solution was incubated at 37 C for 42 h with gentle and constant shaking. Binding assays were carried out as described previously.[24] [^{125}I]IMPY (6-iodo-2-(4′-dimethylamino)phenyl-imidazo[1,2]pyridine) with 2200 Ci/mmol specific activity and greater than 95% radiochemical purity was prepared using the standard iododestannylation reaction as described previously.[15] Binding assays were carried out in 12 75 mm borosilicate glass tubes. A mixture containing 50 μL of test compound (0.2 pM–400 μM in 10% EtOH), 50 μL of [^{125}I]IMPY (0.02 nM diluted in 10%EtOH), 50 μL of Aβ42 aggregates, and 850 μL of 10% ethanol was incubated at room temperature for 3 h. The mixture was then filtered through Whatman GF/B filters using a Brandel M-24 cell harvester, and the filters containing the bound ^{125}I ligand were placed in a gamma counter (Aloka, ARC-380). Values for the half-maximal inhibitory concentration (IC_{50}) were determined from displacement curves of three independent experiments using GraphPad Prism 4.0, and those for the inhibition constant (K_i) were calculated using the Cheng–Prusoff equation.[25]

4.4. Neuropathological staining of model mouse brain sections

The experiments with animals were conducted in accordance with our institutional guidelines and were approved by Nagasaki University Animal Care Committee. The Tg2576 transgenic mice (female, 28-month-old) and wild-type mice (female, 28-month-old) were used as the Alzheimer's model and control mice, respectively. After the mice were sacrificed by decapitation, the brains were immediately removed and frozen in powdered dry ice. The frozen blocks were sliced into serial sections, 10 μm thick. Each slide was incubated with a 50% EtOH solution (100 μM) of compounds 3 and 4 for 30 min. The sections were washed in 50% EtOH for 1 min two times, and examined using a microscope (Nikon Eclipse 80i) equipped with a UV-1A filter set (excitation, 365–375 nm; diachronic mirror, 400 nm; longpass filter, 400 nm). Thereafter, the serial sections were also stained with thioflavin S, a pathological dye commonly used for staining Aβ plaques in the brain, and examined using a microscope (Nikon Eclipse 80i) equipped with a B-2A filter set (excitation, 450–480 nm; diachronic mirror, 505 nm; longpass filter, 520 nm).

4.5. Determination of partition coefficient determination

Partition coefficients were measured by mixing [^{125}I]3 and [^{125}I]4 with 1.5 mL each of 1-octanol and buffer (0.1 M phosphate, pH 7.4) in a test tube. The test tube was vortexed for 20 s three times. Two weighed samples (1 mL each) from the 1-octanol and buffer layers were measured for radioactivity with a gamma counter. The partition coefficient was determined by calculating the ratio of cpm/1 mL of 1-octanol to that of the buffer.

4.6. In vivo biodistribution in normal mice

A saline solution (100 μL) of radiolabeled agents (0.2–0.4 μCi) containing ethanol (10 μL) was injected intravenously directly into the tail of ddY mice (5-week-old, 22–25 g). The mice were sacrificed at various time points postinjection. The organs of interest were removed and weighed, and radioactivity was measured with an automatic gamma counter (Aloka, ARC-380).

Acknowledgments

This study was supported by the Program for Promotion of Fundamental Studies in Health Sciences of the National Institute of Biomedical Innovation (NIBIO) and a Health Labour Sciences Research Grant.

References and notes

1. Klunk, W. E. Neurobiol. Aging 1998, 19, 145.
2. Hardy, J.; Selkoe, D. J. Science 2002, 297, 353.
3. Mathis, C. A.; Lopresti, B. J.; Klunk, W. E. Nucl. Med. Biol. 2007, 34, 809.
4. Mathis, C. A.; Wang, Y.; Klunk, W. E. Curr. Pharm. Des. 2004, 10, 1469.
5. Nordberg, A. Lancet Neurol. 2004, 3, 519.
6. Mathis, C. A.; Wang, Y.; Holt, D. P.; Huang, G. F.; Debnath, M. L.; Klunk, W. E. J. Med. Chem. 2003, 46, 2740.
7. Klunk, W. E.; Engler, H.; Nordberg, A.; Wang, Y.; Blomqvist, G.; Holt, D. P.; Bergstrom, M.; Savitcheva, I.; Huang, G. F.; Estrada, S.; Ausen, B.; Debnath, M. L.; Barletta, J.; Price, J. C.; Sandell, J.; Lopresti, B. J.; Wall, A.; Koivisto, P.; Antoni, G.; Mathis, C. A.; Langstrom, B. Ann. Neurol. 2004, 55, 306.
8. Ono, M.; Wilson, A.; Norbrega, J.; Westaway, D.; Verhoeff, P.; Zhuang, Z. P.; Kung, M. P.; Kung, H. F. Nucl. Med. Biol. 2003, 30, 565.
9. Verhoeff, N. P.; Wilson, A. A.; Takeshita, S.; Trop, L.; Hussey, D.; Singh, K.; Kung, H. F.; Kung, M. P.; Houle, S. Am. J. Geriatr. Psychiatry 2004, 12, 584.
10. Rowe, C. C.; Ackerman, U.; Browne, W.; Mulligan, R.; Pike, K. L.; O'Keefe, G.; Tochon-Danguy, H.; Chan, G.; Berlangieri, S. U.; Jones, G.; Dickinson-Rowe, K. L.; Kung, H. P.; Zhang, W.; Kung, M. P.; Skovronsky, D.; Dyrks, T.; Holl, G.; Krause, S.; Friebe, M.; Lehman, L.; Lindemann, S.; Dinkelborg, L. M.; Masters, C. L.; Villemagne, V. L. Lancet Neurol. 2008, 7, 129.
11. Kudo, Y.; Okamura, N.; Furumoto, S.; Tashiro, M.; Furukawa, K.; Maruyama, M.; Itoh, M.; Iwata, R.; Yanai, K.; Arai, H. J. Nucl. Med. 2007, 48, 553.
12. Agdeppa, E. D.; Kepe, V.; Liu, J.; Flores-Torres, S.; Satyamurthy, N.; Petric, A.; Cole, G. M.; Small, C. W.; Huang, S. C.; Barrio, J. R. J. Neurosci. 2001, 21, RC189.
13. Shoghi-Jadid, K.; Small, G. W.; Agdeppa, E. D.; Kepe, V.; Ercoli, L. M.; Siddarth, P.; Read, S.; Satyamurthy, N.; Petric, A.; Huang, S. C.; Barrio, J. R. Am. J. Geriatr. Psychiatry 2002, 10, 24.
14. Small, G. W.; Kepe, V.; Ercoli, L. M.; Siddarth, P.; Bookheimer, S. Y.; Miller, K. J.; Lavretsky, H.; Burggren, A. C.; Cole, G. M.; Vinters, H. V.; Thompson, P. M.; Huang, S. C.; Satyamurthy, N.; Phelps, M. E.; Barrio, J. R. N. Engl. J. Med. 2006, 355, 2652.
15. Kung, M. P.; Hou, C.; Zhuang, Z. P.; Zhang, B.; Skovronsky, D.; Trojanowski, J. Q.; Lee, V. M.; Kung, H. F. Brain Res. 2002, 956, 202.
16. Zhuang, Z. P.; Kung, M. P.; Wilson, A.; Lee, C. W.; Plossl, K.; Hou, C.; Holtzman, D. M.; Kung, H. F. J. Med. Chem. 2003, 46, 237.
17. Newberg, A. B.; Wintering, N. A.; Plossl, K.; Hochold, J.; Stabin, M. G.; Watson, M.; Skovronsky, D.; Clark, C. M.; Kung, M. P.; Kung, H. F. J. Nucl. Med. 2006, 47, 748.
18. Newberg, A. B.; Wintering, N. A.; Clark, C. M.; Plossl, K.; Skovronsky, D.; Seibyl, J. P.; Kung, M. P.; Kung, H. F. J. Nucl. Med. 2006, 47, 78.
19. Ono, M.; Haratake, M.; Saji, H.; Nakayama, M. Bioorg. Med. Chem. 2008, 16, 6867.
20. Neaterov, E. E.; Skoch, J.; Hyman, B. T.; Klunk, W. E.; Bacskai, B. J.; Swager, T. M. Angew. Chem. Int. Ed. 2005, 44, 5452.
21. Chabdra, R.; Kung, M. P.; Kung, H. F. Bioorg. Med. Chem. Lett. 2006, 16, 1350.
22. Qu, W.; Kung, M. P.; Hou, C.; Oya, S.; Kung, H. F. J. Med. Chem. 2007, 50, 3380.
23. Dabiti, M.; Salehi, P.; Baghbanzadeh, M.; Bahramnejad, M. Tetrahedron Lett. 2006, 47, 6983.
24. Kung, M. P.; Hou, C.; Zhuang, Z. P.; Skovronsky, D.; Kung, H. F. Brain Res. 2004, 1025, 98.
25. Cheng, Y.; Prusoff, W. H. Biochem. Pharmacol. 1973, 22, 3099.